


RESEARCH

Open Access



Biomimetic GBM-targeted drug delivery system boosting ferroptosis for immunotherapy of orthotopic drug-resistant GBM

Bao Liu^{1†}, Qifeng Ji^{1†}, Ying Cheng¹, Miao Liu¹, Bangle Zhang¹, Qibing Mei¹, Daozhou Liu^{1*} and Siyuan Zhou^{1,2*} 

Abstract

Background: Clinical studies have shown that the efficacy of programmed cell death receptor-1/programmed cell death ligand-1 (PD-1/PD-L1) inhibitors on glioblastoma (GBM) is much lower than what is expected because of the low immunogenicity of GBM. Ferroptosis of cancer cells can induce the maturation of dendritic cells (DC cells) and increase the activity of T cell. The activated T cells release IFN- γ , which subsequently induces the ferroptosis of cancer cells. Thus, the aim of this paper is to set up a new GBM-targeted drug delivery system (Fe_3O_4 -siPD-L1@M_{BV2}) to boost ferroptosis for immunotherapy of drug-resistant GBM.

Results: Fe_3O_4 -siPD-L1@M_{BV2} significantly increased the accumulation of siPD-L1 and Fe^{2+} in orthotopic drug-resistant GBM tissue in mice. Fe_3O_4 -siPD-L1@M_{BV2} markedly decreased the protein expression of PD-L1 and increased the ratio between effector T cells and regulatory T cells in orthotopic drug-resistant GBM tissue. Moreover, Fe_3O_4 -siPD-L1@M_{BV2} induced ferroptosis of GBM cells and maturation of DC cell, and it also increased the ratio between M1-type microglia and M2-type microglia in orthotopic drug-resistant GBM tissue. Finally, the growth of orthotopic drug-resistant GBM in mice was significantly inhibited by Fe_3O_4 -siPD-L1@M_{BV2}.

Conclusion: The mutual cascade amplification effect between ferroptosis and immune reactivation induced by Fe_3O_4 -siPD-L1@M_{BV2} significantly inhibited the growth of orthotopic drug-resistant GBM and prolonged the survival time of orthotopic drug-resistant GBM mice.

Keywords: Drug-resistant glioblastoma, siPD-L1, Ferroptosis, Immunotherapy, Glioblastoma, Microglia

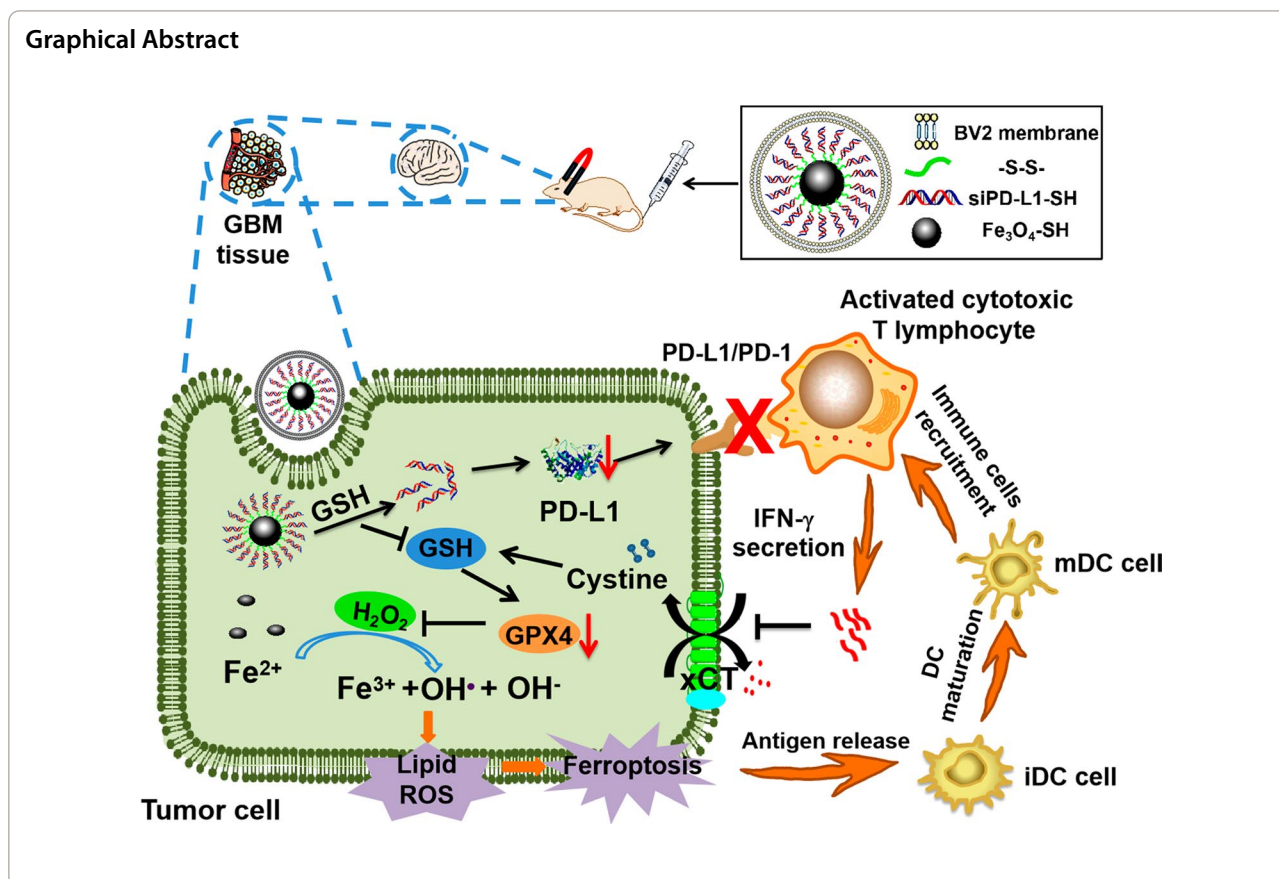
*Correspondence: ldzhnhxh@163.com; zhousy@fmmu.edu.cn

[†]Bao Liu and Qifeng Ji have contributed to the work equally

¹ Department of Pharmaceutics, School of Pharmacy, Air Force Medical University, Changle West Road 169, Xi'an 710032, Shaanxi, China
Full list of author information is available at the end of the article



© The Author(s) 2022. **Open Access** This article is licensed under a Creative Commons Attribution 4.0 International License, which permits use, sharing, adaptation, distribution and reproduction in any medium or format, as long as you give appropriate credit to the original author(s) and the source, provide a link to the Creative Commons licence, and indicate if changes were made. The images or other third party material in this article are included in the article's Creative Commons licence, unless indicated otherwise in a credit line to the material. If material is not included in the article's Creative Commons licence and your intended use is not permitted by statutory regulation or exceeds the permitted use, you will need to obtain permission directly from the copyright holder. To view a copy of this licence, visit <http://creativecommons.org/licenses/by/4.0/>. The Creative Commons Public Domain Dedication waiver (<http://creativecommons.org/publicdomain/zero/1.0/>) applies to the data made available in this article, unless otherwise stated in a credit line to the data.



Background

Glioblastoma (GBM) is an aggressive intracranial malignant tumor with high mortality and morbidity, accounting for 80% of malignant tumors in central nervous system (CNS). The overall median survival for GBM patients is only about 15 months [1, 2]. At present, surgical resection followed by radiotherapy and temozolomide (TMZ) chemotherapy is considered to be the basic treatment for patients with newly diagnosed GBM [3–5]. However, it is frustrating that long-term use of TMZ in GBM patients inevitably leads to the overexpression of O⁶-methylguanine DNA methyltransferase (MGMT) in GBM cells, which results in the resistance of GBM cells to TMZ. Subsequently, the efficacy of TMZ is significantly reduced or even lost [6, 7]. Therefore, it is an urgent need to find new treatment methods for TMZ-resistant GBM.

Immunotherapy, a very promising cancer treatment method, inhibits tumor growth and metastasis by inducing systemic and sustained immune response [8]. However, the efficacy of immunotherapy on GBM is much lower than what is expected. This is resulted from the following reasons. Firstly, as compared with other cancer such as non-small cell lung cancer, GBM in most cases shows a lower tumor mutational burden [9], resulting in

lower immunogenicity of GBM cells and less recruitment of effector T cells (T_{eff} cell) in GBM tissue [10]. Secondly, GBM cells usually recruit regulatory T cell (T_{reg} cell) into GBM tissue by secreting chemokines such as colony stimulating factor 1 (CSF1), C-X-C Motif Chemokine Ligand 12 (CXCL12), C-X-C Motif Chemokine Ligand 1 (CXCL1) and granulocyte-macrophage colony stimulating factor (GM-CSF) [11]. T_{reg} cell inhibits the function of T_{eff} cell, subsequently reducing the generation of interleukin-2 (IL-2) and interferon- γ (IFN- γ) [12, 13]. Finally, GBM cells are able to polarize anti-tumor M1 type microglia/macrophage into the immunosuppressive M2 type microglia/macrophage by secreting immunomodulatory cytokines [14, 15]. M2 type microglia/macrophage also inhibits the function of T_{eff} cell and promotes the progression of GBM by secreting cytokines such as interleukin-6 (IL-6), interleukin-10 (IL-10) and C-C Motif Chemokine Ligand 2 (CCL2) [16].

Ferroptosis is a form of iron-dependent cell death. The essences of ferroptosis are the over-load of Fe²⁺, depletion of glutathione (GSH) and the decrease of glutathione peroxidase (GPX4) [17, 18]. Lipid oxides cannot be metabolized through GPX4. Subsequently, a large number of hydroxyl radicals are produced through Fenton

reaction, leading to lipid peroxidation in cancer cells. This finally results in cancer cell death [19, 20]. Many studies have shown that ferroptosis also leads to the maturation of DC cells in cancer tissue in vivo, and the matured DC cells present antigen to T lymphocytes to activated T_{eff} [21, 22]. Moreover, PD-1/PD-L1 inhibitor is able to activate T_{eff} cell to secrete IFN- γ [23]. IFN- γ secreted by activated T_{eff} cell inhibits the cysteine transporter (xCT) and subsequently prevents the cysteine from being taken up by cancer cells, resulting in the reduction of GSH synthesis in cancer cells. Then, ferroptosis is significantly enhanced in turn [24–26]. In theory, ferroptosis inducer and PD-1/PD-L1 inhibitor can mutually enhance each efficacy when they are simultaneously used to treat GBM.

siRNA shows high specificity and low toxicity in cancer treatment [27]. It has potential application value to interfere PD-L1 protein synthesis in drug-resistant GBM cells by using siPD-L1. However, lack of suitable siPD-L1 delivery vector and easy degradation of siPD-L1 in blood circulation are the main obstacles that limit the application of siPD-L1 in the treatment of GBM [28, 29]. As compared with other carriers, Fe_3O_4 nanoparticle is a promising siPD-L1 carrier [30]. Firstly, Fe_3O_4 nanoparticle displays good biocompatibility and biodegradability, and it is easily available. Fe_3O_4 nanoparticle has been approved for clinic use by the Food and Drug Administration (FDA) [31]. Secondly, Fe_3O_4 nanoparticle significantly increases the intracellular iron content especially Fe^{2+} [32, 33], which provides sufficient substrate for ferroptosis in drug-resistant GBM cells. Last, Fe_3O_4 nanoparticle shows super paramagnetism, which allows it to be directed delivery by an external magnetic field [34]. However, Fe_3O_4 nanoparticle is difficult to cross blood–brain barrier (BBB) [35, 36]. Recent studies have shown that GBM tissue can recruit microglia by secreting chemokines such as C-X3-C motif chemokine ligand 1 (CX3CL1) and CSF-1 [37–39]. In theory, microglia membrane coated Fe_3O_4 nanoparticle can be recruited to drug-resistant GBM.

In this study, disulfide bonds were used to connect thiolated siPD-L1 and thiolated Fe_3O_4 nanoparticles to increase the stability of siPD-L1 in blood circulation. Fe_3O_4 nanoparticles connected with siPD-L1 (Fe_3O_4 -siPD-L1) are further coated with microglial membrane ($M_{\text{BV}2}$) to form a biomimetic brain-targeted nanoparticle Fe_3O_4 -siPD-L1@ $M_{\text{BV}2}$. After Fe_3O_4 -siPD-L1@ $M_{\text{BV}2}$ was taken up by orthotopic drug-resistant GBM cells, the disulfide bond between Fe_3O_4 nanoparticles and siPD-L1 was broken by intracellular GSH, releasing siPD-L1 and inhibiting the protein expression of PD-L1 in orthotopic drug-resistant GBM cells [40]. Subsequently, T_{eff} cell was activated to enhance the killing effect on drug-resistant GBM cell [41]. At the

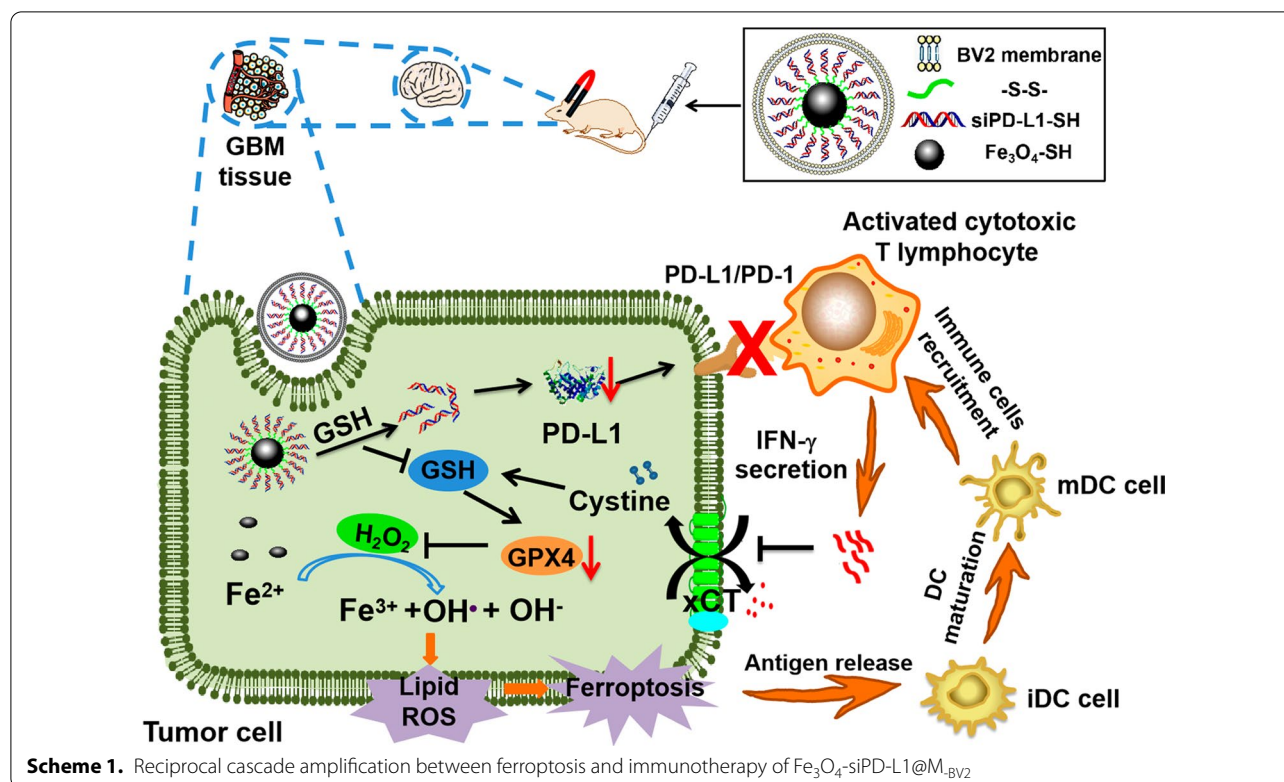
same time, Fe_3O_4 -siPD-L1@ $M_{\text{BV}2}$ facilitated the ferroptosis of drug-resistant GBM cells, which further activated T_{eff} cell by improving the maturation of DC cells. Moreover, activated T_{eff} cell enhanced the ferroptosis of drug-resistant GBM cells in turn by secreting IFN- γ . Finally, there forms a cascade amplification effect between ferroptosis and immune activation in orthotopic drug-resistant GBM tissue (Scheme 1).

Materials and methods

Materials

Thiolated Fe_3O_4 nanoparticle was bought from Ruixibio (Xi'an, China). Thiolated siPD-L1 (5'-GAAGGGAAA UGCUGCCCUUTT-3'; 5'-AAGGGCAUUUCCCUU CTT-3') and cyanine5 labeled siPD-L1 were obtained from GenePharma (Shanghai, China). PD-L1 antibody, GPX4 antibody, xCT antibody, clusters of differentiation 31 (CD31) antibody, clusters of differentiation 44 (CD44) antibody, E-cadherin antibody, N-cadherin antibody, matrix metalloproteinases-9 (MMP-9) antibody, CX3CL1 antibody, colony-stimulating factor 1 receptor (CSF-1R) antibody, clusters of differentiation16/32 (CD16/32) antibody, clusters of differentiation 206 (CD206) antibody, ionized calcium binding adaptor molecule 1 (Iba-1) antibody were bought from Abcam (London, England). CSF-1 antibody and C-X3-C motif chemokine receptor 1 (CX3CR1) antibody were bought from Proteintech (Beijing, China). β -actin antibody were bought from Affinity (Colorado, USA). GM-CSF was bought from Peprotech (Suzhou, China). Anti-mouse clusters of differentiation 11 c-allophycocyanin (CD11c-APC), anti-mouse clusters of differentiation 80-fluorescein (CD80-FITC), anti-mouse clusters of differentiation86-phycoerythrin (CD86-PE), anti-mouse clusters of differentiation 3-allophycocyanin (CD3-APC), anti-mouse clusters of differentiation 8-fluorescein isothiocyanate (CD8-FITC), anti-mouse interferon- γ -phycoerythrin-sulfo-cyanine7 (IFN- γ -PE-Cy7), anti-mouse clusters of differentiation4-phycoerythrin-sulfo-cyanine7 (CD4-PE-Cy7), anti-mouse clusters of differentiation 25-fluorescein isothiocyanate (CD25-FITC), anti-mouse forkhead box p3-phycoerythrin (FoxP3-PE) were obtained from Biolegend (California, USA). Enzyme linked immunosorbent assay (ELISA) kits were obtained from Cloud-Clone corp (Wuhan, China). GSH detection kit and H_2O_2 detection kit were bought from Solarbio (Beijing, China). Reactive oxygen species (ROS) detection kit was bought from Bestbio (Shanghai, China). Boron difluoride pyrrole fluorescent dyes-C11 (BODIPY-C11) staining solution was bought from ThermoFisher (Massachusetts, USA).

GL261 cells, HT-22 cells, BV2 cells, RAW264.7 cells and bEnd3 cells were purchased from CytoBiotech (Xi'an, China). TMZ-resistant GL261 cells were induced in our



lab. 6 weeks old C57 mice and 8 weeks old Sprague-Dawley (SD) male rats were provided by the Experimental Animal Center of Air Force Medical University (Xi'an, China).

Extraction of BV2 cell membrane

BV2 cells in logarithmic growth phase were collected and mixed with 3 mL low-osmotic lysate and 30 μL protease inhibitor. Then, BV2 cells suspension was immersed into liquid nitrogen. After BV2 cells suspension was frozen and thawed for 3 times, the cell lysate was centrifuged for 10 min at 4 $^{\circ}\text{C}$ (14,000 $\times g$). The supernatant was discarded, and 3 mL sterilized deionized water was added into precipitate. The mixture was performed ultrasound for 2 min, and supernatant was collected by centrifuging mixture for 20 min at 4 $^{\circ}\text{C}$ (14,000 $\times g$). Then BV2 cell membrane (M_{BV2}) was obtained by lyophilizing the supernatant.

Preparation of $\text{Fe}_3\text{O}_4\text{-siPD-L1@M}_{\text{BV2}}$

Thiolated siPD-L1 (150 μL , 0.264 mg/mL), H_2O_2 (30%, 55 μL) and thiolated Fe_3O_4 nanoparticles (120 μL , 5 mg/mL) were added into enzyme-free EP tube, and the mixture was stirred for 1 h at room temperature to connect siPD-L1 with Fe_3O_4 nanoparticles by disulfide bond. The reaction mixture was centrifuged for 10 min at 4

$^{\circ}\text{C}$ (9000 $\times g$), and the supernatant was discarded. The precipitate was washed with DEPC water for 6 times to completely remove free siPD-L1. After that, precipitate was re-suspended into PBS buffer to get $\text{Fe}_3\text{O}_4\text{-siPD-L1}$ suspension. The mass ratio between thiolated Fe_3O_4 and thiolated siPD-L1 was optimized by agarose gel electrophoresis. Scramble siPD-L1 was used to prepare $\text{Fe}_3\text{O}_4\text{-siNC}$ nanoparticle by using the same method in the preparation of $\text{Fe}_3\text{O}_4\text{-siPD-L1}$. Finally, 3 mL sterilized deionized water containing 10 mg M_{BV2} was added into $\text{Fe}_3\text{O}_4\text{-siPD-L1}$ suspension. After being performed ultrasonic for 1 min, the mixture solution was incubated at 37 $^{\circ}\text{C}$ for 10 min. The mixture solution was extruded through 0.4 μm polycarbonate membrane for 21 times to obtain $\text{Fe}_3\text{O}_4\text{-siPD-L1@M}_{\text{BV2}}$. $\text{Fe}_3\text{O}_4\text{-FAM}$ was prepared by reacting $\text{Fe}_3\text{O}_4\text{-siPD-L1}$ with maleimide modified carboxyfluorescein (FAM-MAL). To prepare $\text{Fe}_3\text{O}_4\text{-FAM@M}_{\text{BV2}}$, M_{BV2} was coated on the surface of $\text{Fe}_3\text{O}_4\text{-FAM}$ by using the same method in the preparation of $\text{Fe}_3\text{O}_4\text{-siPD-L1@M}_{\text{BV2}}$.

Characterization of $\text{Fe}_3\text{O}_4\text{-siPD-L1@M}_{\text{BV2}}$

Firstly, the morphology and element composition of $\text{Fe}_3\text{O}_4\text{-siPD-L1@M}_{\text{BV2}}$ were investigated by field emission transmission electron microscopy (TEM, FEI Talos F200X, Super-X, ThermoFisher, USA). Particle size, zeta potential and the stability of Fe_3O_4 nanoparticles and

$\text{Fe}_3\text{O}_4\text{-siPD-L1@M}_{\text{BV2}}$ in deionized water, phosphate buffer solution (PBS) and fetal bovine serum (FBS, 10%) were determined by dynamic laser particle size analyzer (Delsa Nano C, Beckman, USA). $\text{Fe}_3\text{O}_4\text{-siPD-L1@M}_{\text{BV2}}$ dispersion was placed at 37 °C in a constant temperature and humidity incubator. After $\text{Fe}_3\text{O}_4\text{-siPD-L1}$ was labeled by FAM and M_{BV2} was labeled by DiI, the membrane structure of $\text{Fe}_3\text{O}_4\text{-siPD-L1@M}_{\text{BV2}}$ was observed by laser scanning confocal microscope (LSCM, Nikon, Japan). The proteins maintained in $\text{Fe}_3\text{O}_4\text{-siPD-L1@M}_{\text{BV2}}$ were observed by SDS-PAGE [42]. Besides, proteins such as CX3CR1, CSF-1R, CX3CL1 and CSF-1 in $\text{Fe}_3\text{O}_4\text{-siPD-L1@M}_{\text{BV2}}$ were detected by western blot [37]. The hemolysis of $\text{Fe}_3\text{O}_4\text{-siPD-L1@M}_{\text{BV2}}$ was investigated by using rat erythrocytes [43]. The release of siPD-L1 from $\text{Fe}_3\text{O}_4\text{-siPD-L1@M}_{\text{BV2}}$ in GSH-containing solution was observed by gel retardation assay [44]. The stability of $\text{Fe}_3\text{O}_4\text{-siPD-L1@M}_{\text{BV2}}$ in RNase A-containing buffer was observed by gel retardation assay.

The selective uptake of $\text{Fe}_3\text{O}_4\text{-FAM@M}_{\text{BV2}}$ by GL261/TR cell, HT-22 cell, BV2 cell and RAW264.7 cell

GL261/TR cells, HT-22 cells, BV2 cells and RAW264.7 cells in logarithmic growth phase were separately inoculated into different 24-well plates containing cover glass at density of 2×10^5 cells/mL and incubated at 37 °C for 24 h. Four cover glass inoculated with different cells were transferred into one well of 6-well plate, and 2 mL of fresh serum-free dulbecco's modified eagle medium (DMEM) containing $\text{Fe}_3\text{O}_4\text{-FAM@M}_{\text{BV2}}$ (the equivalent Fe_3O_4 concentration was 200 $\mu\text{g/mL}$) was added into each well. $\text{Fe}_3\text{O}_4\text{-FAM}$ was used as control. The cells were cultured for 1, 2 and 4 h, respectively. (1) The cells were collected and re-suspend in PBS. The uptake of $\text{Fe}_3\text{O}_4\text{-FAM@M}_{\text{BV2}}$ by GL261/TR cell, HT-22 cell, BV2 cell and RAW264.7 cell was detected by flow cytometer (Beckman, A00-1-1102, USA). (2) The cell culture medium was discarded, and the cells were fixed with 4% paraformaldehyde for 10 min. The cells were washed with PBS for 3 times. Then cells were stained with 4',6-diamidino-2-phenylindole (DAPI) solution (0.5 $\mu\text{g/mL}$) for 10 min. After the cells were washed with PBS for 3 times, the uptake of $\text{Fe}_3\text{O}_4\text{-FAM@M}_{\text{BV2}}$ by GL261/TR cell, HT-22 cell, BV2 cell and RAW264.7 cell was observed by LSCM.

The uptake mechanism of $\text{Fe}_3\text{O}_4\text{-FAM@M}_{\text{BV2}}$ by GL261/TR cell

(1) Fresh serum-free DMEM containing $\text{Fe}_3\text{O}_4\text{-FAM@M}_{\text{BV2}}$ (the equivalent Fe_3O_4 concentration was 200 $\mu\text{g/mL}$) was co-incubated with CX3CR1 antibody (1 $\mu\text{g/mL}$) for 2 h at 37 °C, and then the mixture was added into a 24-well plate pre-inoculated with GL261/TR cells on a cover glass. The

cell was culture at 37 °C for 4 h. (2) Fresh serum-free DMEM containing CX3CL1 antibody (1 $\mu\text{g/mL}$) was added into a 24-well plate pre-inoculated with GL261/TR cells on a cover glass. After co-incubation at 37 °C for 2 h, fresh serum-free DMEM containing $\text{Fe}_3\text{O}_4\text{-FAM@M}_{\text{BV2}}$ (the equivalent Fe_3O_4 concentration was 200 $\mu\text{g/mL}$) was added into cell culture medium, and cell was cultured at 37 °C for 4 h. (3) Chlorpromazine solution (10 $\mu\text{g/mL}$), colchicine solution (800 $\mu\text{g/mL}$), methyl- β -cyclodextrin solution (5 $\mu\text{g/mL}$), and 2-deoxy-D-glucose (900 $\mu\text{g/mL}$) were added into 24-well plates pre-inoculated with GL261/TR cells on a cover glass. The cell was incubated at 37 °C for 2 h, and then fresh serum-free DMEM containing $\text{Fe}_3\text{O}_4\text{-FAM@M}_{\text{BV2}}$ (equivalent Fe_3O_4 concentration was 200 $\mu\text{g/mL}$) was added into cell culture medium. The cell was cultured at 37 °C for 4 h. (4) The GL261/TR cell on a cover glass was incubated at 4 °C for 1 h, and then fresh serum-free DMEM containing $\text{Fe}_3\text{O}_4\text{-FAM@M}_{\text{BV2}}$ (4 °C, equivalent Fe_3O_4 concentration was 200 $\mu\text{g/mL}$) was added into cell culture medium. The cell was cultured at 4 °C for 4 h. After that, the cells were collected and re-suspend in PBS. The uptake of $\text{Fe}_3\text{O}_4\text{-FAM@M}_{\text{BV2}}$ by GL261/TR cell, HT-22 cell, BV2 cell and RAW264.7 cell was detected by flow cytometer. Besides, the cells were fixed with 4% paraformaldehyde for 10 min. The cells were washed with PBS for 3 times. Then cells were stained with DAPI solution (0.5 $\mu\text{g/mL}$) for 10 min. After the cells were washed with PBS for 3 times, the uptake of $\text{Fe}_3\text{O}_4\text{-FAM@M}_{\text{BV2}}$ by GL261/TR cells was observed by LSCM.

The silencing effect of $\text{Fe}_3\text{O}_4\text{-siPD-L1@M}_{\text{BV2}}$ on PD-L1 protein in GL261 cells and GL261/TR cells

GL261 cells and GL261/TR cells in logarithmic growth phase were inoculated into 6-well plates at density of 5×10^5 cells/mL per well and incubated at 37 °C for 24 h. The culture medium was replaced with fresh serum-free DMEM medium containing $\text{Fe}_3\text{O}_4\text{-siNC}$ (150 nM scramble siPD-L1), siPD-L1@Lipo2000 (150 nM siPD-L1), $\text{Fe}_3\text{O}_4\text{-siPD-L1}$ (150 nM siPD-L1) and $\text{Fe}_3\text{O}_4\text{-siPD-L1@M}_{\text{BV2}}$ (150 nM siPD-L1) and cultured for 48 h. Then, cells were collected and proteins were extracted. Western blot was used to investigate the silencing effect of $\text{Fe}_3\text{O}_4\text{-siPD-L1@M}_{\text{BV2}}$ on PD-L1 protein in GL261 cells and GL261/TR cells.

Effects of $\text{Fe}_3\text{O}_4\text{-siPD-L1@M}_{\text{BV2}}$ on the viability of GL261/TR cells

GL261/TR cells in logarithmic growth phase were inoculated into 96-well plates at density of 3×10^4 cells/mL per well and incubated at 37 °C for 24 h. The culture medium was replaced with serum-free DMEM medium containing Fe_3O_4 , $\text{Fe}_3\text{O}_4\text{-siPD-L1}$ and $\text{Fe}_3\text{O}_4\text{-siPD-L1@M}_{\text{BV2}}$ (equivalent Fe_3O_4 concentration was 10, 20, 50, 100, 200 $\mu\text{g/mL}$), and the cells were incubated at 37 °C for

48 h. 20 μL MTT solution (5 mg/mL) was added into each well and incubated at 37 °C for 4 h. The culture medium in well was discarded, and 150 μL DMSO was added into each well. The absorbance of each well was measured at 490 nm by enzyme linked immune-analyzer (Bio-Rad Laboratories, Inc. California, USA), and the cell survival rate was calculated.

MTT method was also used to illuminate whether $\text{Fe}_3\text{O}_4\text{-siPD-L1@M}_{\text{BV2}}$ could induce ferroptosis. Briefly, GL261/TR cells in logarithmic growth phase were inoculated into 96-well plates at density of 3×10^4 cells/mL per well and incubated at 37 °C for 24 h. The culture medium was replaced with fresh serum-free DMEM medium containing $\text{Fe}_3\text{O}_4\text{-siPD-L1@M}_{\text{BV2}}$ (equivalent Fe_3O_4 concentration was 10, 20, 50, 100, 200 $\mu\text{g/mL}$) at the present of IFN- γ (10 ng/mL), ferostatin1 (Fer-1, 10 μM) and deferoxamine (DFO, 100 μM). The cells were incubated at 37 °C for 48 h. 20 μL MTT solution (5 mg/mL) was added into each well, and cells were incubated at 37 °C for 4 h. The culture medium in well was discarded, and 150 μL DMSO was added into each well. The absorbance of each well was measured at 490 nm by enzyme linked immune-analyzer, and the cell survival rate was calculated.

Staining of living and dead cells

GL261/TR cells in logarithmic growth phase were inoculated into 6-well plates at density of 5×10^5 cells/mL per well and incubated at 37 °C for 24 h. The culture medium was replaced with fresh serum-free DMEM medium containing $\text{Fe}_3\text{O}_4\text{-siNC}$, Fe_3O_4 , $\text{Fe}_3\text{O}_4\text{-siPD-L1}$, $\text{Fe}_3\text{O}_4\text{-siPD-L1@M}_{\text{BV2}}$, $\text{Fe}_3\text{O}_4\text{-siPD-L1@M}_{\text{BV2}} + \text{Fer-1}$, $\text{Fe}_3\text{O}_4\text{-siPD-L1@M}_{\text{BV2}} + \text{DFO}$ and $\text{Fe}_3\text{O}_4\text{-siPD-L1@M}_{\text{BV2}} + \text{IFN-}\gamma$. The equivalent Fe_3O_4 concentration was 200 $\mu\text{g/mL}$. The concentration of IFN- γ , Fer-1 and DFO was 10 ng/mL, 10 μM and 100 μM , respectively. Cells were incubated at 37 °C for 48 h. The cells were collected and washed twice with $1 \times$ assay buffer. Then, 1 mL staining solution was used to re-suspended cells, and cell suspension was incubated at 37 °C for 20 min. After centrifugation ($2000 \times g$, 5 min), the supernatant was discarded, and the cells were re-suspended in PBS. The living and dead cells was observed under a fluorescence microscope (Nikon, Japan).

Effects of $\text{Fe}_3\text{O}_4\text{-siPD-L1@M}_{\text{BV2}}$ on expression of GPX4 and xCT in GL261/TR cells

GL261/TR cells in logarithmic growth phase were inoculated into 6-well plates at density of 5×10^5 cells/mL per well and incubated at 37 °C for 24 h. The culture medium was replaced with fresh serum-free DMEM medium containing IFN- γ , Fe_3O_4 , $\text{Fe}_3\text{O}_4\text{-siPD-L1}$, $\text{Fe}_3\text{O}_4\text{-siPD-L1@M}_{\text{BV2}}$, $\text{Fe}_3\text{O}_4\text{-siPD-L1@M}_{\text{BV2}} + \text{Fer-1}$, $\text{Fe}_3\text{O}_4\text{-siPD-L1@M}_{\text{BV2}} + \text{DFO}$ and $\text{Fe}_3\text{O}_4\text{-siPD-L1@M}_{\text{BV2}} + \text{IFN-}\gamma$. The equivalent Fe_3O_4

concentration was 200 $\mu\text{g/mL}$. The concentration of IFN- γ , Fer-1 and DFO was 10 ng/mL, 10 μM and 100 μM , respectively. The cells were incubated at 37 °C for 48 h. Then, cells were collected and proteins were extracted. Western blot was used to detect protein expression of GPX4 and xCT in GL261/TR cells.

Effects of $\text{Fe}_3\text{O}_4\text{-siPD-L1@M}_{\text{BV2}}$ on GSH and H_2O_2 level in GL261/TR cells

GL261/TR cells in logarithmic growth phase were inoculated into cell culture bottle (25 cm^2) at density of 5×10^5 cells/mL and incubated at 37 °C for 24 h. The culture medium was replaced with fresh serum-free DMEM medium containing $\text{Fe}_3\text{O}_4\text{-siNC}$, Fe_3O_4 , $\text{Fe}_3\text{O}_4\text{-siPD-L1}$, $\text{Fe}_3\text{O}_4\text{-siPD-L1@M}_{\text{BV2}}$, $\text{Fe}_3\text{O}_4\text{-siPD-L1@M}_{\text{BV2}} + \text{Fer-1}$, $\text{Fe}_3\text{O}_4\text{-siPD-L1@M}_{\text{BV2}} + \text{DFO}$ and $\text{Fe}_3\text{O}_4\text{-siPD-L1@M}_{\text{BV2}} + \text{IFN-}\gamma$. The equivalent Fe_3O_4 concentration was 200 $\mu\text{g/mL}$. The concentration of IFN- γ , Fer-1 and DFO was 10 ng/mL, 10 μM and 100 μM , respectively. After the cells were incubated at 37 °C for 48 h, the cells were collected. The cells were frozen and thawed for 3 times. The cell lysate was centrifuged for 10 min ($8000 \times g$, 15 min), and the supernatant was collected. The concentration of GSH and H_2O_2 in the supernatant was respectively detected by using GSH and H_2O_2 detection kit.

Effects of $\text{Fe}_3\text{O}_4\text{-siPD-L1@M}_{\text{BV2}}$ on ROS and lipid peroxidation level in GL261/TR cells

GL261/TR cells in logarithmic growth phase were inoculated into 6-well plates at density of 5×10^5 cells/mL per well and incubated at 37 °C for 24 h. The culture medium was replaced with fresh serum-free DMEM medium containing $\text{Fe}_3\text{O}_4\text{-siNC}$, Fe_3O_4 , $\text{Fe}_3\text{O}_4\text{-siPD-L1}$, $\text{Fe}_3\text{O}_4\text{-siPD-L1@M}_{\text{BV2}}$, $\text{Fe}_3\text{O}_4\text{-siPD-L1@M}_{\text{BV2}} + \text{Fer-1}$, $\text{Fe}_3\text{O}_4\text{-siPD-L1@M}_{\text{BV2}} + \text{DFO}$ and $\text{Fe}_3\text{O}_4\text{-siPD-L1@M}_{\text{BV2}} + \text{IFN-}\gamma$. The equivalent Fe_3O_4 concentration was 200 $\mu\text{g/mL}$. The concentration of IFN- γ , Fer-1 and DFO was 10 ng/mL, 10 μM and 100 μM , respectively. The cells were incubated at 37 °C for 24 h. The cells were washed with serum-free DMEM medium for 3 times. (1) For detection ROS level, 1 mL of DHE dye solution (diluted 1000 times with serum-free DMEM medium) was added into each well. The cells were incubated at 37 °C for 1 h. Then cells were fixed with 4% paraformaldehyde and stained with DAPI solution (0.5 $\mu\text{g/mL}$). After the cells were washed with PBS for 3 times, the ROS in GL261/TR cells was observed under fluorescence microscope. (2) For detection lipid peroxidation level, 1 mL of C11 BODIPY dye solution (diluted 1000 times with serum-free DMEM medium) was added into each well. The cells were incubated at 37 °C for 0.5 h. Then cells were fixed with 4% paraformaldehyde and

stained with DAPI solution (0.5 $\mu\text{g}/\text{mL}$). After the cells were washed with PBS for 3 times, the lipid peroxidation (LPO) in GL261/TR cells was observed under fluorescence microscope.

Effects of Fe_3O_4 -siPD-L1@M_{BV2} on DC cell maturation in vitro

Femur and tibia of C57 male mice were isolated and immersed in 75% ethanol for 5 min. Then, femur and tibia were immersed in serum-free Roswell Park Memorial Institute 1640 medium (RPMI1640). The ends of the femur and tibia were cut off with scissors, and the bone marrow cells were rinsed out from the femur and tibia by using serum-free RPMI1640 medium. The culture medium containing bone marrow cells was filtered (70 μm , BioFIL). The filtrate was centrifuged (1000 \times g, 3 min), and supernatant was discarded. The cells were re-suspended with red blood cell lysate (R1010, Solarbio). After the cell suspension was placed at room temperature for 1.5 min, RPMI1640 complete medium was added. The supernatant was discarded by centrifugation (1000 \times g, 3 min), and the cells were re-suspended by RPMI1640 complete medium containing GM-CSF (20 ng/mL). The cells were inoculated into 6-well plates at a density of 3×10^6 cells/mL in each well (1 mL). 3 days later, 1 mL of RPMI1640 complete medium containing GM-CSF (20 ng/mL) was added into each well and cultured for another 2 days.

2 mL of cell culture medium containing Fe_3O_4 , Fe_3O_4 -siNC, Fe_3O_4 -siPD-L1, Fe_3O_4 -siPD-L1@M_{BV2}, Fe_3O_4 -siPD-L1@M_{BV2}+IFN- γ , Fe_3O_4 -siPD-L1@M_{BV2}+DFO, and Fe_3O_4 -siPD-L1@M_{BV2}+Fer-1 (the equivalent Fe_3O_4 concentration was 200 $\mu\text{g}/\text{mL}$, the concentration of IFN- γ , Fer-1 and DFO was 10 ng/mL, 10 μM and 100 μM , respectively) was added into transwell donor chamber planted GL261/TR cells, respectively. After incubation for 6 h, donor chamber was transferred to a 6-well plate inoculated with DC cells at the bottom and cultured for 24 h. DC cells were collected and re-suspended with PBS. APC-CD11c antibody (0.2 mg/mL), FITC-CD80 antibody (0.5 mg/mL) and PE-CD86 antibody (0.2 mg/mL) were added into cell culture medium, and cell was incubated at 4 $^\circ\text{C}$ for 30 min in dark room. The cells were collected and re-suspended with 200 μL PBS. The proportion of CD11c⁺, CD86⁺ and CD80⁺ DCs was detected by flow cytometer.

Efficiency of Fe_3O_4 -siPD-L1@M_{BV2} transport across the in vitro BBB

bEnd3 cells in the logarithmic growth phase were inoculated into the transwell donor chamber at a density of

5×10^5 cells/mL per well. Serum-free DMEM medium was added into the recipient chamber, and bEnd3 cells were cultured at 37 $^\circ\text{C}$. The complete medium was replaced every two days. The resistance between transwell donor chamber and recipient chamber was measured by using a resistance meter. When the resistance value exceeded 200 Ω/cm^2 , the in vitro BBB model was regarded to be successfully established [45].

The transwell donor chamber was transferred into a 24-well plate inoculated with GL261/TR cells at the bottom. 400 μL of fresh serum-free DMEM medium containing Fe_3O_4 -FAM, Fe_3O_4 -FAM@M_{BV2} were added into donor chamber (the equivalent Fe_3O_4 concentration was 200 $\mu\text{g}/\text{mL}$). 0.8 mL of DMEM medium was added into recipient chamber. At the same time, a group with a magnet outside of the 24-well plates (Fe_3O_4 -FAM@M_{BV2} + magnet) was designed. After cell was incubated for 1 h, 4 h, 8 h and 12 h, the resistance values between transwell donor chamber and recipient chamber were measured to evaluate the integrity of the in vitro BBB model. The fluorescence intensity of the medium in recipient chamber was determined by fluorescence spectrophotometer (HITACHI, F-2700, Japan), and the in vitro BBB transmission efficiency of Fe_3O_4 -FAM@M_{BV2} was calculated. Finally, GL261/TR cells at the bottom of recipient chamber were collected and re-suspended in PBS. The uptake of Fe_3O_4 -FAM@M_{BV2} by GL261/TR cell was detected by flow cytometer. Besides, GL261/TR cells at the bottom of recipient chamber were fixed with 4% paraformaldehyde and then were stained with DAPI solution (0.5 $\mu\text{g}/\text{mL}$). After the cells were washed with PBS for 3 times, the uptake of Fe_3O_4 -FAM@M_{BV2} by GL261/TR cells was observed by LSCM after it penetrated in vitro BBB.

Effects of CX3CL1 and CSF-1 on the transport of Fe_3O_4 -siPD-L1@M_{BV2} across the in vitro BBB

(1) After the successful establishment of the in vitro BBB model, the transwell donor chamber was transferred into a 24-well plates inoculated with GL261/TR cells at the bottom, and 800 μL fresh serum-free DMEM was added into recipient chamber. (2) After the successful establishment of the in vitro BBB model, the transwell donor chamber was transferred into a 24-well plates without GL261/TR cells at the bottom, and 800 μL fresh serum-free DMEM containing CX3CL1 (200 ng/mL) or CSF-1 (100 ng/mL) was added into recipient chamber. After that, 400 μL of fresh serum-free DMEM containing Fe_3O_4 -FAM@M_{BV2} was added into transwell donor chamber (the equivalent Fe_3O_4 concentration was 200 $\mu\text{g}/\text{mL}$). The 24-well plates without GL261/TR cell and chemokine was used as the control. After incubation

for 4 h, the fluorescence intensity of the culture medium in recipient chamber was measured by fluorescence spectrophotometer.

After the successful establishment of the *in vitro* BBB model, transwell donor chamber was transferred into a 24-well plate inoculated with GL261/TR cells. (1) $\text{Fe}_3\text{O}_4\text{-FAM@M}_{\text{BV2}}$ (the equivalent Fe_3O_4 concentration was 200 $\mu\text{g}/\text{mL}$) was incubated with fresh serum-free DMEM containing CX3CR1 or CSF-1R antibody for 2 h at 37 °C, and then they were added into transwell donor chamber. 800 μL of serum-free DMEM was added into recipient chamber. (2) Fresh serum-free DMEM containing CX3CL1 or CSF-1 antibody was added into recipient chamber and incubated with GL261/TR cells at 37 °C for 2 h. After that, 400 μL of fresh serum-free DMEM containing $\text{Fe}_3\text{O}_4\text{-FAM@M}_{\text{BV2}}$ was added into donor chamber (the equivalent Fe_3O_4 concentration was 200 $\mu\text{g}/\text{mL}$). The concentration of antibody was 1 $\mu\text{g}/\text{mL}$. $\text{Fe}_3\text{O}_4\text{-FAM@M}_{\text{BV2}}$ without incubation with antibody was used as control. After incubation for 4 h, the fluorescence intensity of the culture medium in recipient chamber was measured by fluorescence spectrophotometer.

Establishment of orthotopic drug-resistant GBM model in mice

Luciferase expressed GL261/TR cell (Luc-GL261/TR) in logarithmic growth phase were prepared as $2 \times 10^7/\text{mL}$ cell suspension. C57 mice were anesthetized and fixed on the operation table, and a micro-injector was inserted into the skull at the right front 2 mm of the intersection of sagittal suture and coronal suture. 5 μL of cell suspension was slowly injected into the brain with the brain stereotactic locator to establish orthotopic drug-resistant GBM model *in vivo*.

Distribution and pharmacokinetics of $\text{Fe}_3\text{O}_4\text{-siPD-L1@M}_{\text{BV2}}$ in orthotopic drug-resistant GBM mice

On the 10th day after plantation of Luc-GL261/TR cell, luciferase substrate was intraperitoneally injected (150 mg/kg). 5 min post injection, the mice were anesthetized with isoflurane. The GBM growth was observed by bioluminescence imaging (IVIS Lumina II, Caliper, USA), and the mice that the volume of orthotopic drug-resistant GBM did not meet the requirements were excluded.

The GBM-bearing mice were randomly divided into 4 groups. siPD-L1, $\text{Fe}_3\text{O}_4\text{-siPD-L1}$, $\text{Fe}_3\text{O}_4\text{-siPD-L1@M}_{\text{BV2}}$ and $\text{Fe}_3\text{O}_4\text{-siPD-L1@M}_{\text{BV2}}$ + magnet (Additional file 1: Fig. S1) were injected into GBM-bearing mice via tail vein (siPD-L1 was labeled by Cy5, equivalent siPD-L1 dose was 0.3 mg/kg). 6 h and 12 h later, *in vivo* bioluminescence imaging was used to observe the fluorescence distribution in the whole body of orthotopic drug-resistant GBM mice. The integrated brain targeting

efficiency was calculated with the following equation. The integrated brain targeting efficiency = (fluorescence intensity in brain organ/fluorescence intensity in whole body) \times 100%. Blood, brain, heart, liver, spleen, lung and kidney tissues were collected at 0.08, 1, 3, 6, 12 and 24 h after drug administration. *In vivo* bioluminescence imaging was used to observe the distribution of Cy5 labeled $\text{Fe}_3\text{O}_4\text{-siPD-L1@M}_{\text{BV2}}$ in brain, heart, liver, spleen, lung and kidney. The brain tissue was immobilized in 4% paraformaldehyde for 24 h. After tissue was sectioned, DAPI was used to label the nuclei, CD31 antibody was used to label the tumor vessels, and the distribution of $\text{Fe}_3\text{O}_4\text{-siPD-L1@M}_{\text{BV2}}$ in drug-resistant glioma tissue was observed by LSCM. Fluorescence spectrophotometer was used to detect the Cy5 labeled $\text{Fe}_3\text{O}_4\text{-siPD-L1@M}_{\text{BV2}}$ concentration in plasma samples. The GBM tissue was isolation from brain tissue. The GBM tissue and normal brain tissue were respectively ground with 0.8 mL PBS buffer in an ice bath, and the tissue homogenate was centrifuged (9000 \times g, 15 min, 4 °C). The precipitation and supernatant were separated. (1) The concentration of Cy5 labeled $\text{Fe}_3\text{O}_4\text{-siPD-L1@M}_{\text{BV2}}$ in extracellular fluid of brain tissue was detected by fluorescence spectrophotometer. (2) The precipitation was ground with 0.6 mL RIPA cell lysate. The cell lysate was centrifuged (9000 \times g, 20 min, 4 °C). The intracellular Cy5 labeled $\text{Fe}_3\text{O}_4\text{-siPD-L1@M}_{\text{BV2}}$ concentration in GBM tissue was detected by fluorescence spectrophotometer. (3) The intracellular content of Fe^{2+} in GBM tissue was detected by using Perls stain kit. The precipitation was ground with 0.6 mL RIPA cell lysate. The cell lysate was centrifuged (9000 \times g, 20 min, 4 °C). 0.5 mL of supernatant was added into 0.5 mL $\text{NH}_4\text{Fe}(\text{SO}_4)_2$ solution. The above mixture solution was shaken at room temperature for 30 min. Then, the absorbance value of mixture solution at 700 nm was detected by using UV spectrophotometer. After that, dilute nitric acid was added into mixture solution, and the absorbance value of mixture solution at 700 nm was detected again by using UV spectrophotometer. The content of Fe^{2+} can be calculated according to the change of absorbance value.

The therapeutic effect of $\text{Fe}_3\text{O}_4\text{-siPD-L1@M}_{\text{BV2}}$ on orthotopic drug-resistant GBM in mice

On the 10th day after plantation of Luc-GL261/TR cell, luciferase substrate was intraperitoneally injected (150 mg/kg). 15 min later, the mice were anesthetized with isoflurane. The GBM growth was observed by bioluminescence imaging, and the mice that the volume of orthotopic drug-resistant GBM did not meet the requirement was excluded.

The GBM-bearing mice were randomly divided into 10 groups: normal saline group, TMZ group (44 mg/

kg), Fe₃O₄ group, Fe₃O₄-siNC group (equivalent siNC dose was 0.3 mg/kg), Fe₃O₄-siPD-L1 group (equivalent siPD-L1 dose was 0.3 mg/kg), Fe₃O₄-siPD-L1@M_{BV2} group (equivalent siPD-L1 dose was 0.3 mg/kg), Fe₃O₄-siPD-L1@M_{BV2} group (equivalent siPD-L1 dose was 1 mg/kg), Fe₃O₄-siNC@M_{BV2} (equivalent siNC dose was 1 mg/kg), Fe₃O₄-siNC@M_{BV2} + magnet (equivalent siNC dose was 1 mg/kg) and Fe₃O₄-siPD-L1@M_{BV2} + magnet group (equivalent siPD-L1 dose was 1 mg/kg). Different formulations were injected into GBM-bearing mice through tail vein once every three days, for a total of 4 times. (1) The body weight and the death of GBM-bearing mice were recorded. The survival curve was drawn, and the median survival time was calculated. (2) On 10, 17, 20 and 23 day after plantation of Luc-GL261/TR cell, the mice were intraperitoneally injected with luciferase substrate (150 mg/kg), the orthotopic GBM growth was observed by *in vivo* bioluminescence imaging. On the 24th day after plantation of Luc-GL261/TR cell, the GBM-bearing mice were sacrificed. Blood of GBM-bearing mice was collected and serum was separated. The contents of alanine aminotransferase (ALT), aspartate aminotransferase (AST), urea nitrogen (BUN) and creatinine (CREA) in serum were detected by automatic biochemical analyzer (Chemray 800, Shenzhen, China). The lymphocytes in orthotopic GBM tissue were isolated. The number of CD11c⁺CD86⁺CD80⁺ cells (mDCs), CD4⁺CD25⁺FoxP3⁺T cells (T_{reg} cell) and CD3⁺CD8⁺IFN-γ⁺T cells (T_{eff} cell) in orthotopic GBM tissue were detected by flow cytometer. The expressions of PD-L1, invasion-related proteins including E-cadherin, N-cadherin, CD44, matrix metalloproteinases-9 (MMP-9), tumor necrosis factor-α (TNF-α), ferroptosis-related proteins including GPX4 and xCT in orthotopic drug-resistant GBM tissue were detected by western blot. The TNF-α, IFN-γ, IL-6, IL-10 and IL-12 level in orthotopic drug-resistant GBM tissue was determined by ELISA kit. *H&E* staining, Ki67 staining and tdT-mediated dUTP nick-end labeling (TUNEL) staining was used to investigate the effects of Fe₃O₄-siPD-L1@M_{BV2} on cell morphology, proliferation and apoptosis in orthotopic drug-resistant GBM tissue. The expression of CD16/32, CD206, Iba-1, GPX4 and PD-L1 in paraffin sections of orthotopic drug-resistant GBM tissue was observed by immunofluorescence staining method. Dihydroethidium (DHE) probe was used to stain ROS in frozen sections of drug-resistant GBM tissue. The content of GSH in orthotopic drug-resistant GBM tissue was determined by GSH detection kit. *H&E* staining was performed on heart, liver, spleen, lung and kidney tissues to investigate the

in vivo toxicity of Fe₃O₄-siPD-L1@M_{BV2} in GBM-bearing mice.

Statistical analysis

All data are expressed as mean ± standard deviation. The statistics analysis of each group was performed by using one-way ANOVA with SPSS 26.0 statistical software. *p* < 0.05 was considered statistically significant.

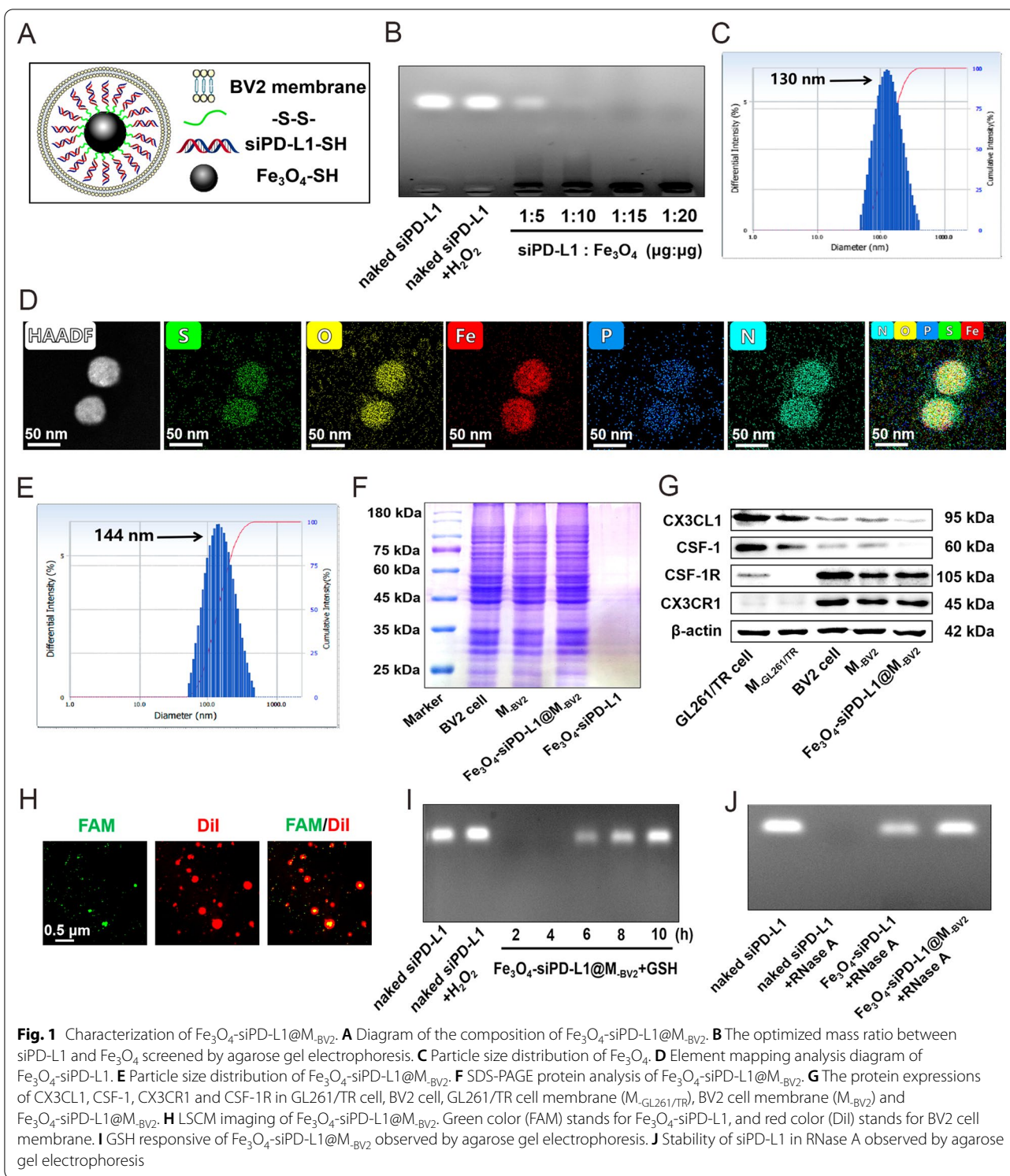
Results

Characterization of Fe₃O₄-siPD-L1@M_{BV2}

The schematic diagram of Fe₃O₄-siPD-L1@M_{BV2} is showing in Fig. 1A. The agarose gel electrophoresis experiment showed that siPD-L1 and Fe₃O₄ were completely connected when mass ratio between siPD-L1 and Fe₃O₄ was 1:15 (Fig. 1B). The average particle size of Fe₃O₄ was 130 nm (Fig. 1C). Mapping results showed that Fe₃O₄ contained O, Fe and S elements. Beside O, Fe and S, Fe₃O₄-siPD-L1 contained N and P elements, indicating that siPD-L1 was successfully connected with Fe₃O₄ (Fig. 1D; Additional file 1: Fig. S2A). The average particle size and zeta potential of Fe₃O₄-siPD-L1@M_{BV2} was 144 nm and -27 mV (Fig. 1E; Additional file 1: Fig. S2B). The protein bands of Fe₃O₄-siPD-L1@M_{BV2} were consistent with that of BV2 cell membrane (M_{BV2}) (Fig. 1F), indicating that the proteins on BV2 cells membrane were well retained in Fe₃O₄-siPD-L1@M_{BV2}. Western blot results indicated that microglial chemokines CX3CL1 and CSF-1 were highly expressed in GL261/TR cells, and their receptors CX3CR1 and CSF-1R were retained in M_{BV2} and Fe₃O₄-siPD-L1@M_{BV2} (Fig. 1G). Moreover, LSCM experiment showed that red color of M_{BV2} was completely merged with green color of Fe₃O₄ (Fig. 1H). The above results demonstrated that M_{BV2} was successfully coated on the surface of Fe₃O₄-siPD-L1. Fe₃O₄-siPD-L1@M_{BV2} remained stable within 7 days in PBS and water, and it was stable within 3 days in 10%FBS (Additional file 1: Fig. S2C). TEM results showed that the appearance of Fe₃O₄ and Fe₃O₄-siPD-L1@M_{BV2} was spherical (Additional file 1: Fig. S2D, E). GSH promoted the release of siPD-L1 from Fe₃O₄-siPD-L1@M_{BV2} in concentration-dependent manner (Fig. 1I). The naked siPD-L1 was rapidly degraded in RNase A solution, while Fe₃O₄-siPD-L1@M_{BV2} protected siPD-L1 from degradation by RNase A (Fig. 1J). Fe₃O₄-siPD-L1@M_{BV2} did not cause hemolysis reaction (Additional file 1: Fig. S2F, G).

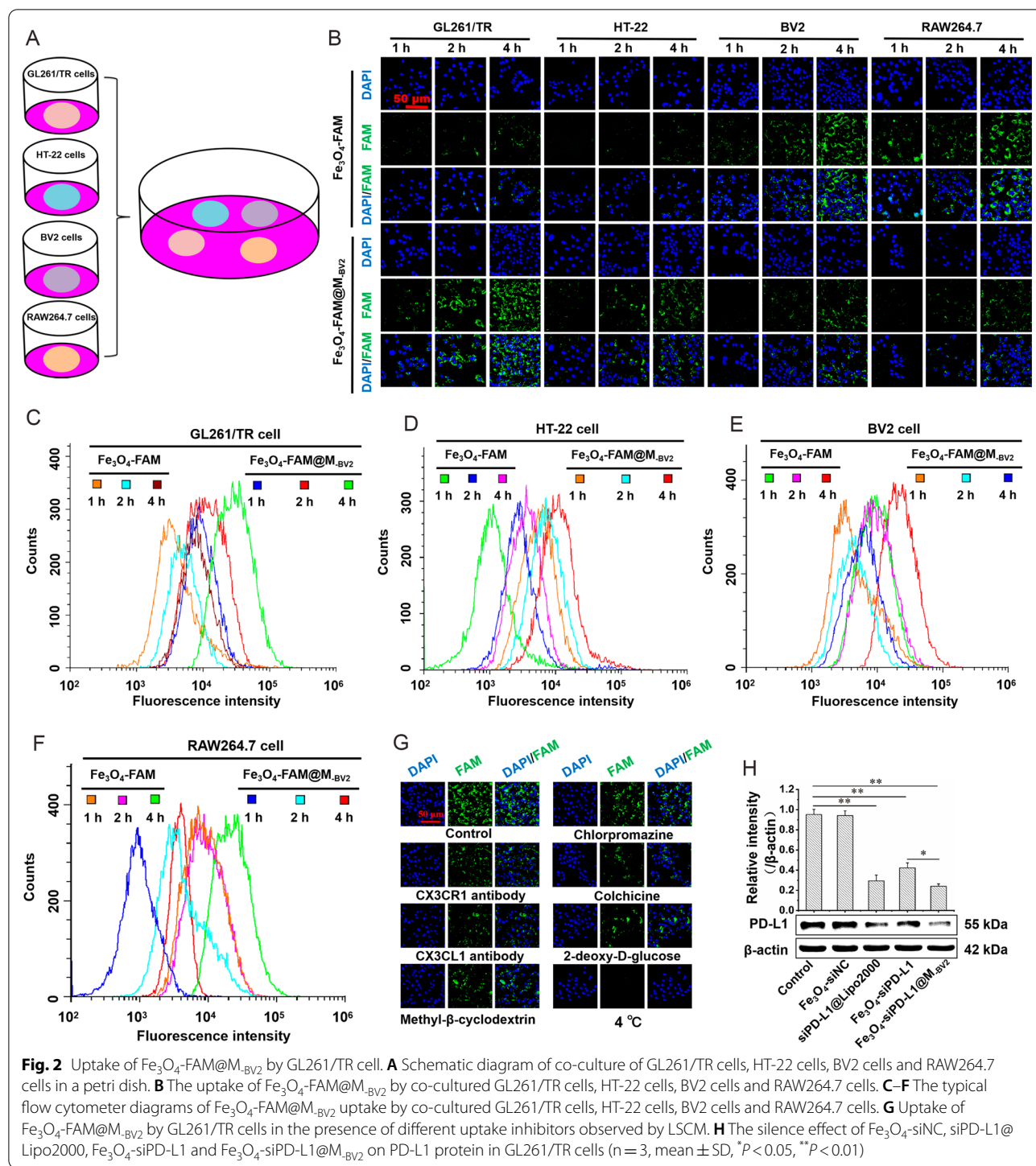
Cellular uptake and gene silence efficiency of Fe₃O₄-FAM@M_{BV2}

GL261/TR cells, HT-22 cells, BV2 cells and RAW264.7 cells at logarithmic growth stage were respectively



planted into 24-well plates containing cover glass at the same density. Cells were incubated at 37 °C for 24 h, the densities of the four cells were basically the same (Additional file 1: Fig. S3). When GL261/TR cells, HT-22

cells, BV2 cells and RAW264.7 cells were co-cultured in a petri dish (Fig. 2A), they took up Fe_3O_4 -FAM@M_{BV2} in a time-dependent manner. BV2 cells and RAW264.7 cells took up more amount of Fe_3O_4 -FAM than



$\text{Fe}_3\text{O}_4\text{-FAM@M}_{\text{BV2}}$. As compared with $\text{Fe}_3\text{O}_4\text{-FAM}$, more amount of $\text{Fe}_3\text{O}_4\text{-FAM@M}_{\text{BV2}}$ was taken up by GL261/TR cells. Moreover, GL261/TR cells took up much more amount of $\text{Fe}_3\text{O}_4\text{-FAM@M}_{\text{BV2}}$ than HT-22 cells did (Fig. 2B–F; Additional file 1: Fig. S4). This indicated that M_{BV2} coating significantly reduced the uptake

of $\text{Fe}_3\text{O}_4\text{-FAM@M}_{\text{BV2}}$ by BV2 cells and RAW264.7 cells. $\text{Fe}_3\text{O}_4\text{-FAM@M}_{\text{BV2}}$ was specifically taken up by GL261/TR cells. Furthermore, low temperature and 2-deoxy-D-glucose pretreatment markedly reduced the uptake of $\text{Fe}_3\text{O}_4\text{-FAM@M}_{\text{BV2}}$ by GL261/TR cells, indicating that the endocytosis of $\text{Fe}_3\text{O}_4\text{-FAM@M}_{\text{BV2}}$ by GL261/TR

TR cells required energy supply. Colchicine significantly inhibited the uptake of $\text{Fe}_3\text{O}_4\text{-FAM@M}_{\text{BV2}}$ by GL261/TR cells, suggesting that $\text{Fe}_3\text{O}_4\text{-FAM@M}_{\text{BV2}}$ was taken by GL261/TR cells mainly through macropinocytosis. CX3CR1 antibody and CX3CL1 antibody also significantly reduced the uptake of $\text{Fe}_3\text{O}_4\text{-FAM@M}_{\text{BV2}}$ by GL261/TR cells, indicating that CX3CR1 and CX3CL1 were involved in the uptake of $\text{Fe}_3\text{O}_4\text{-FAM@M}_{\text{BV2}}$ by GL261/TR cells (Fig. 2G, Additional file 1: Fig. S5). After nanoparticle was taken up by GL261/TR cells, the silence efficiency of siPD-L1@Lipo2000, $\text{Fe}_3\text{O}_4\text{-siPD-L1}$ and $\text{Fe}_3\text{O}_4\text{-siPD-L1@M}_{\text{BV2}}$ on PD-L1 protein in GL261/TR cells were 69.18%, 58.74% and 74.81%, respectively (Fig. 2H). The similar results were observed in GL261 cells (Additional file 1: Fig. S6).

The ferroptosis induced by $\text{Fe}_3\text{O}_4\text{-siPD-L1@M}_{\text{BV2}}$

The essence of ferroptosis is Fenton reaction, which is triggered by Fe^{2+} and H_2O_2 (Fig. 3A). Firstly, MTT assay showed that $\text{Fe}_3\text{O}_4\text{-siPD-L1}$ and $\text{Fe}_3\text{O}_4\text{-siPD-L1@M}_{\text{BV2}}$ significantly reduced the activity of GL261/TR cells in a concentration-dependent manner. As compared with $\text{Fe}_3\text{O}_4\text{-siPD-L1}$, $\text{Fe}_3\text{O}_4\text{-siPD-L1@M}_{\text{BV2}}$ displayed stronger inhibitory effect on the activity of GL261/TR cells (Fig. 3B). In the presence of IFN- γ , the cytotoxicity of $\text{Fe}_3\text{O}_4\text{-siPD-L1@M}_{\text{BV2}}$ on GL261/TR cell was significantly enhanced. However, in the existence of ferroptosis inhibitor such as Fer-1 and DFO, the cytotoxicity of $\text{Fe}_3\text{O}_4\text{-siPD-L1@M}_{\text{BV2}}$ on GL261/TR cell was markedly attenuated (Fig. 3C). The same results were observed by living and dead cells staining experiment (Additional file 1: Fig. S7). The above results confirmed that $\text{Fe}_3\text{O}_4\text{-siPD-L1@M}_{\text{BV2}}$ induced ferroptosis.

Secondly, $\text{Fe}_3\text{O}_4\text{-siPD-L1@M}_{\text{BV2}}$ significantly reduced GSH level in GL261/TR cells. In the existence of IFN- γ , the GSH level in GL261/TR cells was further decreased by $\text{Fe}_3\text{O}_4\text{-siPD-L1@M}_{\text{BV2}}$. However, in the presence of Fer-1 and DFO, the GSH depletion induced by $\text{Fe}_3\text{O}_4\text{-siPD-L1@M}_{\text{BV2}}$ was weakened in GL261/TR cells (Fig. 3D).

Thirdly, Fe_3O_4 had no significant effect on GPX4 protein expression in GL261/TR cells. $\text{Fe}_3\text{O}_4\text{-siPD-L1}$ and $\text{Fe}_3\text{O}_4\text{-siPD-L1@M}_{\text{BV2}}$ significantly reduced the

protein expression of GPX4 in GL261/TR cells (Fig. 3E). In the existence of Fer-1 and DFO, the inhibitory effect of $\text{Fe}_3\text{O}_4\text{-siPD-L1@M}_{\text{BV2}}$ on GPX4 protein expression in GL261/TR cells was weakened. IFN- γ inhibited GPX4 and x-CT protein expression in GL261/TR cells, and the inhibitory effect of $\text{Fe}_3\text{O}_4\text{-siPD-L1@M}_{\text{BV2}}$ on GPX4 protein expression was enhanced in the presence of IFN- γ (Fig. 3F; Additional file 1: Fig. S8).

Finally, $\text{Fe}_3\text{O}_4\text{-siNC}$, $\text{Fe}_3\text{O}_4\text{-siPD-L1}$ and $\text{Fe}_3\text{O}_4\text{-siPD-L1@M}_{\text{BV2}}$ significantly increased ROS, LPO and H_2O_2 level in GL261/TR cells. Moreover, in the presence of IFN- γ , ROS, LPO and H_2O_2 level in GL261/TR cells were further increased by $\text{Fe}_3\text{O}_4\text{-siPD-L1@M}_{\text{BV2}}$. However, in the presence of Fer-1 and DFO, the increase of ROS, LPO and H_2O_2 in GL261/TR cells induced by $\text{Fe}_3\text{O}_4\text{-siPD-L1@M}_{\text{BV2}}$ was attenuated (Fig. 3G–J).

The maturation of DC cell induced by $\text{Fe}_3\text{O}_4\text{-siPD-L1@M}_{\text{BV2}}$ in vitro

Flow cytometer experiment showed that the proportion of $\text{CD11c}^+\text{CD80}^+\text{CD86}^+$ cells in Fe_3O_4 , $\text{Fe}_3\text{O}_4\text{-siPD-L1}$ and $\text{Fe}_3\text{O}_4\text{-siPD-L1@M}_{\text{BV2}}$ treatment groups was 9.67%, 45.26% and 68.2%, respectively, indicating that $\text{Fe}_3\text{O}_4\text{-siPD-L1}$ and $\text{Fe}_3\text{O}_4\text{-siPD-L1@M}_{\text{BV2}}$ significantly promoted the maturation of DC cells in vitro. As compared with $\text{Fe}_3\text{O}_4\text{-siPD-L1}$, $\text{Fe}_3\text{O}_4\text{-siPD-L1@M}_{\text{BV2}}$ facilitated the maturation of DC cells more strongly. In addition, the proportion of $\text{CD11c}^+\text{CD80}^+\text{CD86}^+$ cells in $\text{Fe}_3\text{O}_4\text{-siPD-L1@M}_{\text{BV2}}$ +IFN- γ groups was increased to 77.31%, suggesting the effect of $\text{Fe}_3\text{O}_4\text{-siPD-L1@M}_{\text{BV2}}$ on inducing maturation of DC cell was further enhanced in the presence of IFN- γ . However, the proportion of $\text{CD11c}^+\text{CD80}^+\text{CD86}^+$ cells in $\text{Fe}_3\text{O}_4\text{-siPD-L1@M}_{\text{BV2}}$ +DFO and $\text{Fe}_3\text{O}_4\text{-siPD-L1@M}_{\text{BV2}}$ +Fer-1 groups was 54.4% and 50.21%, respectively. This indicated that ferroptosis inhibitors significantly reduced the maturation of DC cell induced by $\text{Fe}_3\text{O}_4\text{-siPD-L1@M}_{\text{BV2}}$ (Fig. 4).

Transport of $\text{Fe}_3\text{O}_4\text{-FAM@M}_{\text{BV2}}$ across in vitro BBB

Within 12 h when drug is administered, there was no significant difference in resistance values between donor chamber and recipient chamber. It indicated

(See figure on next page.)

Fig. 3 The ferroptosis induced by $\text{Fe}_3\text{O}_4\text{-siPD-L1@M}_{\text{BV2}}$ in GL261/TR cells. **A** Mechanism of ferroptosis. **B** Effect of $\text{Fe}_3\text{O}_4\text{-siPD-L1@M}_{\text{BV2}}$ on the viability of GL261/TR cells. **C** Effect of $\text{Fe}_3\text{O}_4\text{-siPD-L1@M}_{\text{BV2}}$ on the viability of GL261/TR cells in the presence of IFN- γ , Fer-1 and DFO. **D** Effect of $\text{Fe}_3\text{O}_4\text{-siPD-L1@M}_{\text{BV2}}$ on GSH level in GL261/TR cells. **E** Effect of $\text{Fe}_3\text{O}_4\text{-siPD-L1@M}_{\text{BV2}}$ on the protein expression of GPX4 in GL261/TR cells in the presence of Fer-1 and DFO. **F** Effect of $\text{Fe}_3\text{O}_4\text{-siPD-L1@M}_{\text{BV2}}$ on the protein expression of GPX4 in GL261/TR cells in the presence of IFN- γ . **G** Effect of $\text{Fe}_3\text{O}_4\text{-siPD-L1@M}_{\text{BV2}}$ on ROS (marked with DHE, red color) and LPO (marked with BODIPY-C11, green color) level in GL261/TR cells. **H** Statistic analysis of effect of $\text{Fe}_3\text{O}_4\text{-siPD-L1@M}_{\text{BV2}}$ on ROS level in GL261/TR cells. **I** Statistic analysis of effect of $\text{Fe}_3\text{O}_4\text{-siPD-L1@M}_{\text{BV2}}$ on LPO level in GL261/TR cells. **J** Effect of $\text{Fe}_3\text{O}_4\text{-siPD-L1@M}_{\text{BV2}}$ on H_2O_2 level in GL261/TR cells. (n = 3, mean \pm SD, * P < 0.05, ** P < 0.01; ns: no significant difference)

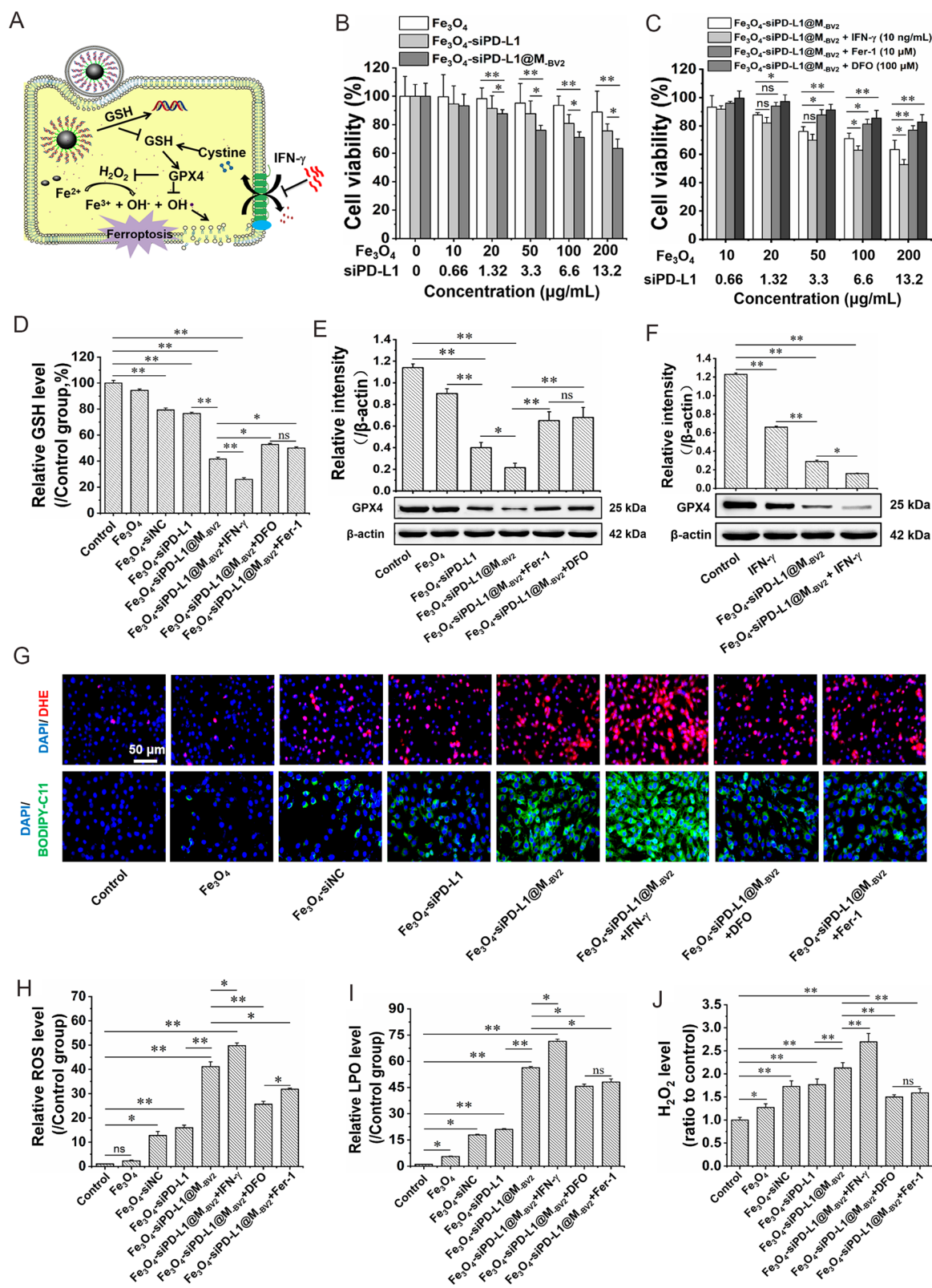
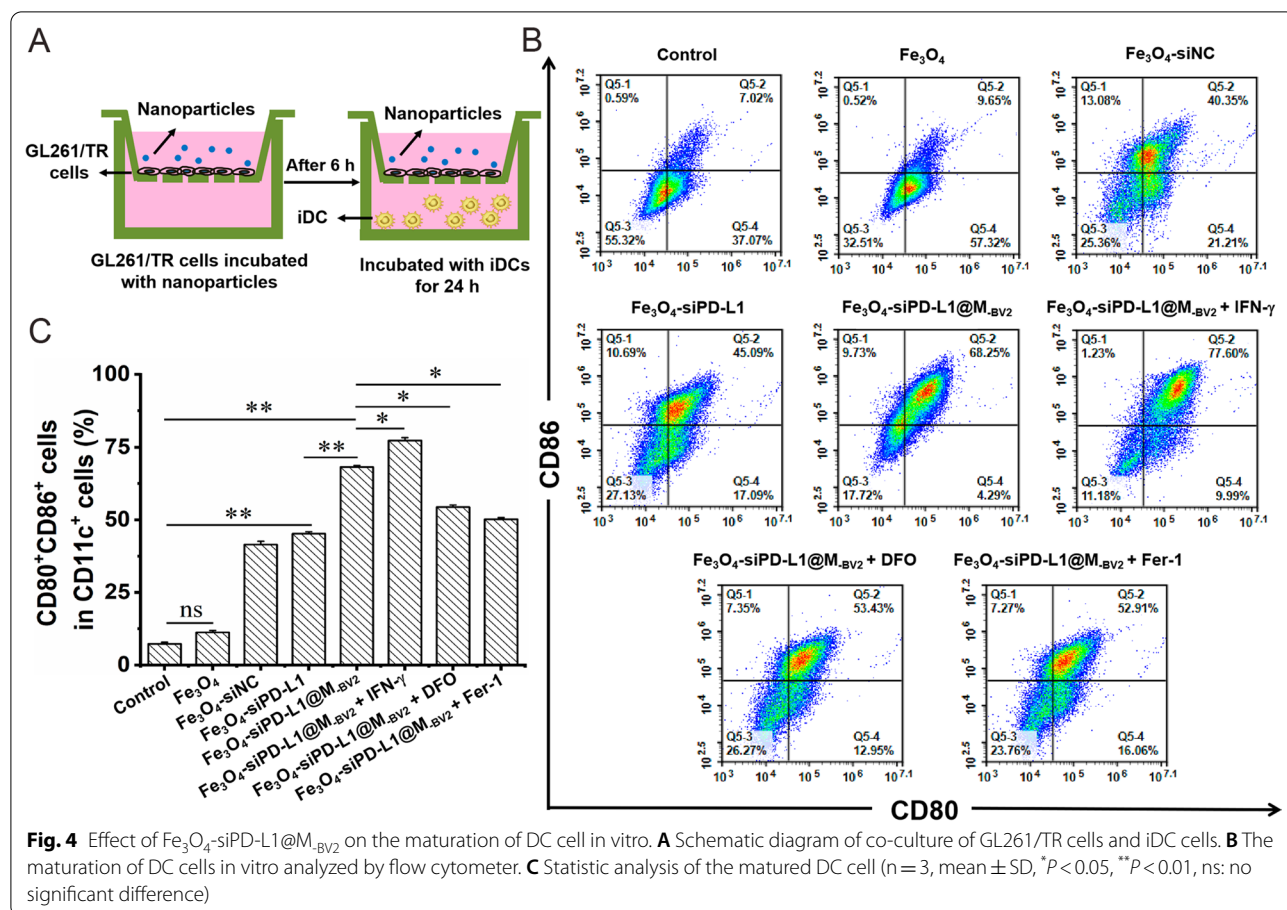


Fig. 3 (See legend on previous page.)

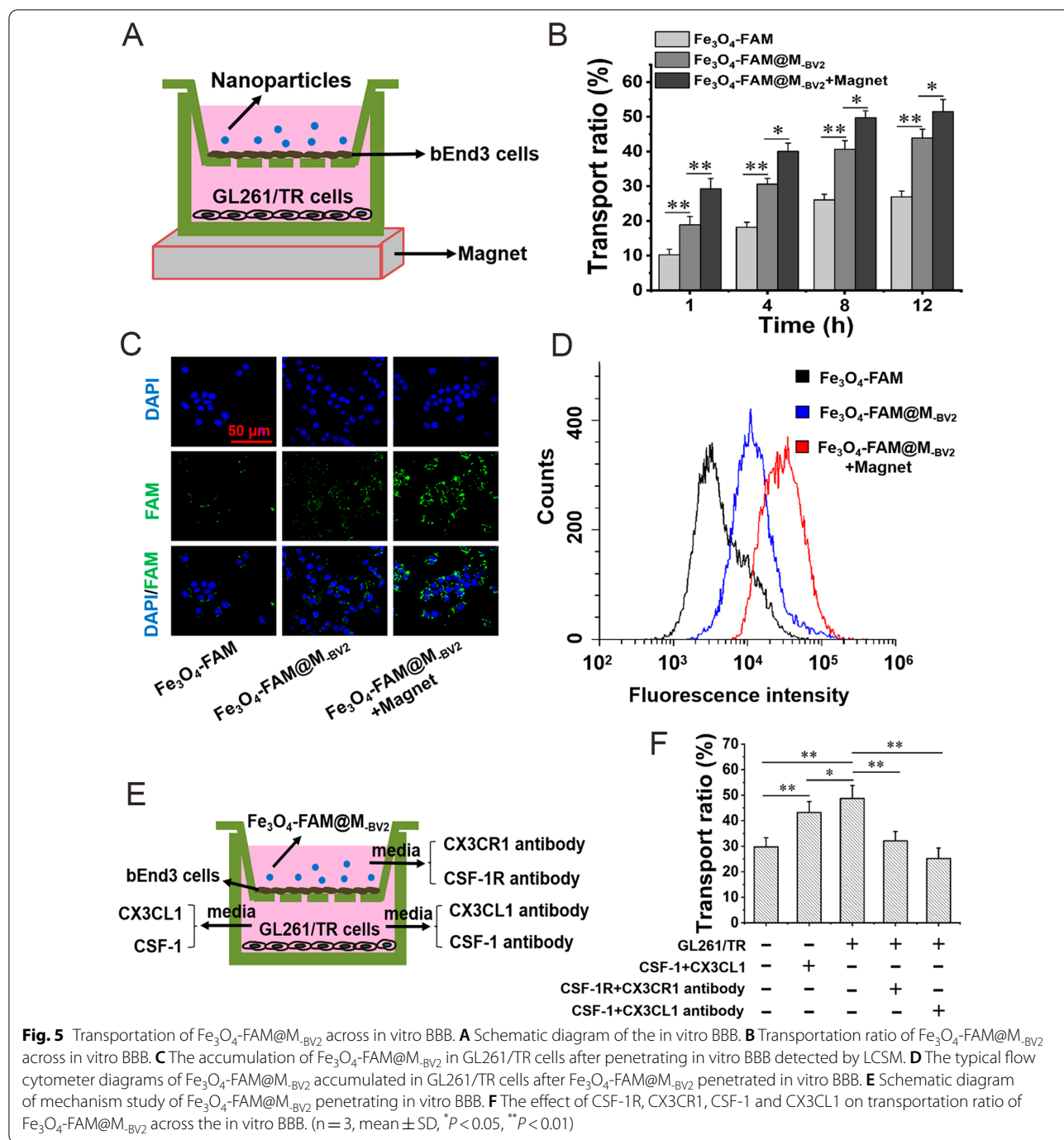


that drug treatment did not damage the integrity of in vitro BBB model (Additional file 1: Fig. S9). As compared with Fe₃O₄-FAM, the transportation ratio of Fe₃O₄-FAM@M-BV₂ across in vitro BBB was significantly higher, and it was further increased in the presence of external magnetic field (Fig. 5A, B). Compared with Fe₃O₄-FAM, the accumulation of Fe₃O₄-FAM@M-BV₂ in GL261/TR cells was significantly increased after it penetrated in vitro BBB. In the presence of external magnetic field, the accumulation of Fe₃O₄-FAM@M-BV₂ in GL261/TR cells was further increased after it penetrated in vitro BBB (Fig. 5C, D, Additional file 1: Fig. S10). Moreover, the transport ratio of Fe₃O₄-FAM@M-BV₂ across in vitro BBB was significantly increased when GL261/TR cells were cultivated in recipient chamber in comparison with that without GL261/TR cells in recipient chamber. This suggested that GL261/TR cells facilitated the transport of Fe₃O₄-FAM@M-BV₂ across in vitro BBB. When there were not GL261/TR cells in recipient chamber, the addition of CSF-1 and CX3CL1 in recipient chamber also significantly increased the transport ratio of Fe₃O₄-FAM@M-BV₂ across in vitro BBB. After CSF-1

antibody and CX3CL1 antibody were added into recipient chamber, the transport ratio of Fe₃O₄-FAM@M-BV₂ across in vitro BBB was significantly reduced. Moreover, when CSF-1R antibody and CX3CR1 antibody were added into donor chamber to block CSF-1R and CX3CR1 on the surface of Fe₃O₄-FAM@M-BV₂, the transport ratio of Fe₃O₄-FAM@M-BV₂ across in vitro BBB was also significantly decreased (Fig. 5E, F).

Distribution and pharmacokinetics of Fe₃O₄-siPD-L1@M-BV₂ in orthotopic drug-resistant GBM mice

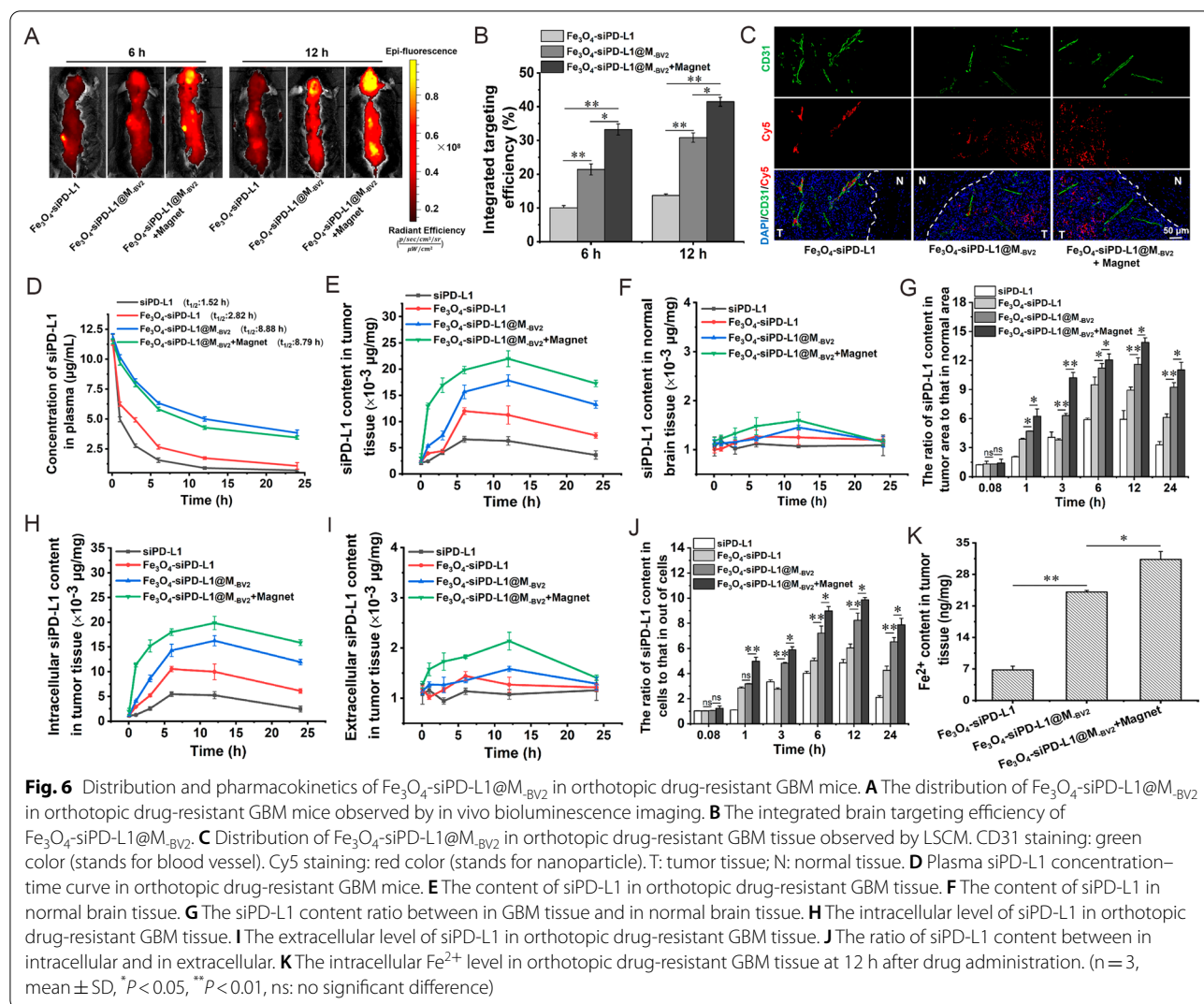
After intravenous administration of Fe₃O₄-siPD-L1@M-BV₂, the distribution of Fe₃O₄-siPD-L1@M-BV₂ in orthotopic drug-resistant GBM mice was observed by in vivo bioluminescence imaging. The results showed that as compared with Fe₃O₄-siPD-L1 group, fluorescence intensity in mice brain in Fe₃O₄-siPD-L1@M-BV₂ group and Fe₃O₄-siPD-L1@M-BV₂ + magnet group was significantly increased. Fe₃O₄-siPD-L1@M-BV₂ + magnet group showed the strongest fluorescence intensity in mice brain (Fig. 6A; Additional file 1: Fig. S11). The integrated brain targeting efficiencies of Fe₃O₄-siPD-L1, Fe₃O₄-siPD-L1@M-BV₂ and Fe₃O₄-siPD-L1@M-BV₂ + magnet group at 12 h



were 13.69%, 30.85% and 41.7%, respectively (Fig. 6B). Results of LSCM showed that a large amount of $\text{Fe}_3\text{O}_4\text{-siPD-L1@M}_{\text{BV2}}$ distributed in orthotopic drug-resistant GBM tissue, and little amount of $\text{Fe}_3\text{O}_4\text{-siPD-L1@M}_{\text{BV2}}$ distributed in the normal brain tissue. Moreover, $\text{Fe}_3\text{O}_4\text{-siPD-L1}$ mainly distributed in the blood vessels, while $\text{Fe}_3\text{O}_4\text{-siPD-L1@M}_{\text{BV2}}$ mainly distributed out of blood vessels in orthotopic drug-resistant GBM

tissue (Fig. 6C), suggesting that $\text{Fe}_3\text{O}_4\text{-siPD-L1@M}_{\text{BV2}}$ penetrated deep region in GBM tissue.

Pharmacokinetic experiment showed that the half-life of siPD-L1 in plasma in naked siPD-L1, $\text{Fe}_3\text{O}_4\text{-siPD-L1}$, $\text{Fe}_3\text{O}_4\text{-siPD-L1@M}_{\text{BV2}}$ and $\text{Fe}_3\text{O}_4\text{-siPD-L1@M}_{\text{BV2}}$ + magnet groups was 1.52 h, 2.82 h, 8.88 h and 8.79 h, respectively (Fig. 6D). After administration of $\text{Fe}_3\text{O}_4\text{-siPD-L1@M}_{\text{BV2}}$ and $\text{Fe}_3\text{O}_4\text{-siPD-L1@M}_{\text{BV2}}$ + magnet, the content of



siPD-L1 in orthotopic drug-resistant GBM tissue increased successively in comparison with naked siPD-L1 and $\text{Fe}_3\text{O}_4\text{-siPD-L1}$. Moreover, the content of siPD-L1 in orthotopic drug-resistant GBM tissue was significantly higher than that in normal brain tissue (Fig. 6E–G). As compared with the $\text{Fe}_3\text{O}_4\text{-siPD-L1}$ group, the intracellular level of siPD-L1 in drug-resistant GBM tissue was significantly increased in $\text{Fe}_3\text{O}_4\text{-siPD-L1@M}_{\text{BV2}}$ group and $\text{Fe}_3\text{O}_4\text{-siPD-L1@M}_{\text{BV2}}$ + magnet group (Fig. 6H–J). The intracellular level of Fe^{2+} in orthotopic drug-resistant GBM tissue was significantly increased in $\text{Fe}_3\text{O}_4\text{-siPD-L1@M}_{\text{BV2}}$ group and $\text{Fe}_3\text{O}_4\text{-siPD-L1@M}_{\text{BV2}}$ + magnet group as compared with that in $\text{Fe}_3\text{O}_4\text{-siPD-L1}$ group (Fig. 6K).

The inhibitory effect of $\text{Fe}_3\text{O}_4\text{-siPD-L1@M}_{\text{BV2}}$ on the growth of orthotopic drug-resistant GBM in mice

In vivo bioluminescence imaging was used to dynamic observe the growth of orthotopic drug-resistant GBM

(Fig. 7A). As compared with normal saline, $\text{Fe}_3\text{O}_4\text{-siNC}$ and $\text{Fe}_3\text{O}_4\text{-siNC@M}_{\text{BV2}}$ significantly inhibited the growth of orthotopic drug-resistant GBM. As compared with $\text{Fe}_3\text{O}_4\text{-siNC}$ and $\text{Fe}_3\text{O}_4\text{-siNC@M}_{\text{BV2}}$, $\text{Fe}_3\text{O}_4\text{-siPD-L1}$ and $\text{Fe}_3\text{O}_4\text{-siPD-L1@M}_{\text{BV2}}$ significantly inhibited the growth of orthotopic drug-resistant GBM. $\text{Fe}_3\text{O}_4\text{-siPD-L1@M}_{\text{BV2}}$ displayed much stronger inhibitory effect on the growth of orthotopic drug-resistant GBM in comparison with $\text{Fe}_3\text{O}_4\text{-siPD-L1}$, suggesting that ferroptosis combined with immunotherapy further inhibited the growth of orthotopic drug-resistant glioma. In addition, in the presence of external magnetic field, the inhibitory effect of $\text{Fe}_3\text{O}_4\text{-siPD-L1@M}_{\text{BV2}}$ on orthotopic drug-resistant GBM was further enhanced (Fig. 7B, C).

On 26th, 28th, 27th, 29th, 32th and 41th day after the plantation of Luc-GL261/TR cell, all normal saline, TMZ, Fe_3O_4 , $\text{Fe}_3\text{O}_4\text{-siNC}$, $\text{Fe}_3\text{O}_4\text{-siPD-L1}$ and low-dose $\text{Fe}_3\text{O}_4\text{-siPD-L1@M}_{\text{BV2}}$ treated orthotopic drug-resistant

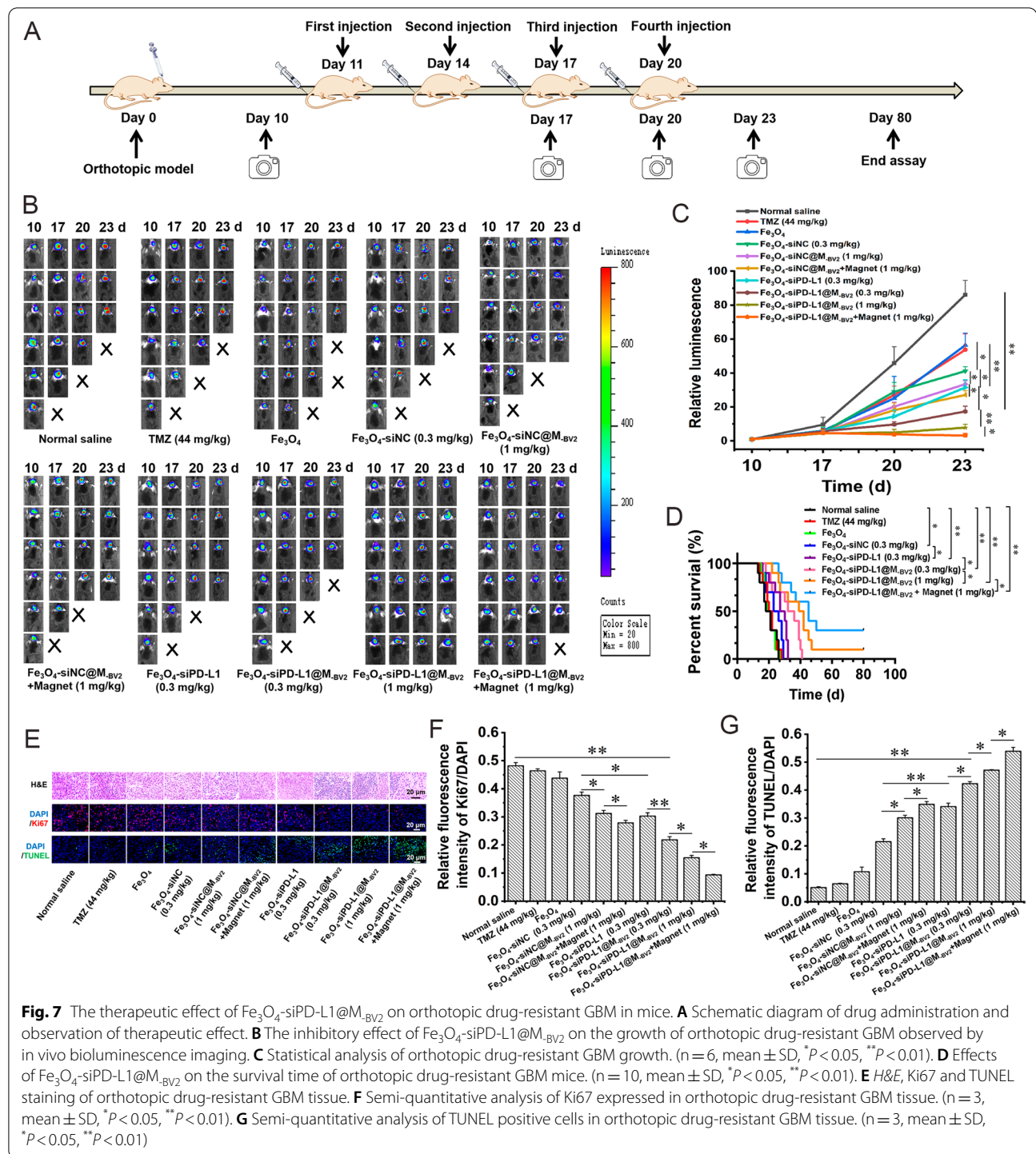


Fig. 7 The therapeutic effect of Fe₃O₄-siPD-L1@M_{BV2} on orthotopic drug-resistant GBM in mice. **A** Schematic diagram of drug administration and observation of therapeutic effect. **B** The inhibitory effect of Fe₃O₄-siPD-L1@M_{BV2} on the growth of orthotopic drug-resistant GBM observed by in vivo bioluminescence imaging. **C** Statistical analysis of orthotopic drug-resistant GBM growth. (n = 6, mean ± SD, *P < 0.05, **P < 0.01). **D** Effects of Fe₃O₄-siPD-L1@M_{BV2} on the survival time of orthotopic drug-resistant GBM mice. (n = 10, mean ± SD, *P < 0.05, **P < 0.01). **E** H&E, Ki67 and TUNEL staining of orthotopic drug-resistant GBM tissue. **F** Semi-quantitative analysis of Ki67 expressed in orthotopic drug-resistant GBM tissue. (n = 3, mean ± SD, *P < 0.05, **P < 0.01). **G** Semi-quantitative analysis of TUNEL positive cells in orthotopic drug-resistant GBM tissue. (n = 3, mean ± SD, *P < 0.05, **P < 0.01)

GBM mice died in succession. However, on 60 days after the plantation of Luc-GL261/TR cell, the survival rate was 10% and 30% in high-dose Fe₃O₄-siPD-L1@M_{BV2} group and high-dose Fe₃O₄-siPD-L1@M_{BV2} + magnet

group, respectively (Fig. 7D). The median survival time of normal saline, TMZ, Fe₃O₄, Fe₃O₄-siNC, Fe₃O₄-siPD-L1, low-dose Fe₃O₄-siPD-L1@M_{BV2}, high-dose Fe₃O₄-siPD-L1@M_{BV2} and high-dose

Fe₃O₄-siPD-L1@M_{BV2} + magnet treated GBM mice was 17.68, 21.39, 18.61, 22.28, 26.94, 31.56, 38.72 and 45.00 days, respectively.

H&E staining of orthotopic drug-resistant GBM tissue presented a long oval shape and a large number of pathological nuclear mitosis in normal saline, TMZ and Fe₃O₄ treated group. Fe₃O₄-siPD-L1@M_{BV2} decreased the number of heteromorphic nuclear cells and nuclear division in orthotopic drug-resistant GBM tissue. The nucleus was regular spherical and the intercellular space became blurred or even disappeared in Fe₃O₄-siPD-L1@M_{BV2} + magnet treated group (Fig. 7E). Moreover, Fe₃O₄-siNC@M_{BV2}, Fe₃O₄-siNC@M_{BV2} + magnet, Fe₃O₄-siPD-L1@M_{BV2} and Fe₃O₄-siPD-L1@M_{BV2} + magnet obviously inhibited Ki67 expression and increased the number of TUNEL positive cells in orthotopic drug-resistant GBM tissue as compared with normal saline, free TMZ and Fe₃O₄ (Fig. 7E–G). These results indicated that Fe₃O₄-siPD-L1@M_{BV2} markedly inhibited proliferation of orthotopic drug-resistant GBM cells and promoted its apoptosis.

The body weight of orthotopic drug-resistant GBM mice in normal saline, TMZ, Fe₃O₄, Fe₃O₄-siNC, Fe₃O₄-siPD-L1 and low-dose Fe₃O₄-siPD-L1@M_{BV2} group decreased gradually. The body weight of orthotopic drug-resistant GBM mice in high-dose Fe₃O₄-siPD-L1@M_{BV2} group and Fe₃O₄-siPD-L1@M_{BV2} + magnet group showed a trend of increasing (Additional file 1: Fig. S12), indicating the growth of orthotopic drug-resistant GBM was markedly blocked by Fe₃O₄-siPD-L1@M_{BV2} and Fe₃O₄-siPD-L1@M_{BV2} + magnet.

Mechanisms of Fe₃O₄-siPD-L1@M_{BV2} on inhibition the growth of orthotopic drug-resistant GBM

Firstly, Fe₃O₄-siPD-L1, Fe₃O₄-siPD-L1@M_{BV2} and Fe₃O₄-siPD-L1@M_{BV2} + magnet significantly increased the protein expression of E-cadherin and decreased the protein expression of TGF-β, MMP-9, CD44 and N-cadherin in orthotopic drug-resistant GBM tissue. (Additional file 1: Fig. S13), indicating Fe₃O₄-siPD-L1@M_{BV2} inhibited the invasion and migration of orthotopic drug-resistant GBM cells through regulating invasion-related protein expression.

Secondly, Fe₃O₄-siPD-L1@M_{BV2} decreased the protein expression of PD-L1, x-CT and GPX4 in orthotopic drug-resistant GBM tissue in dose-dependent manner. As compared with Fe₃O₄-siPD-L1, Fe₃O₄-siPD-L1@M_{BV2} reduced the protein expression of PD-L1, xCT and GPX4 more strongly. The protein expressions of PD-L1, xCT and GPX4 in orthotopic drug-resistant GBM tissue were less in Fe₃O₄-siPD-L1@M_{BV2} + magnet group than that in Fe₃O₄-siPD-L1@M_{BV2} group (Fig. 8A, B). At the same time, immunofluorescence staining was also used to investigate the effects of Fe₃O₄-siPD-L1@M_{BV2} on the protein expression of GPX4 and PD-L1 in orthotopic drug-resistant GBM tissue, and the results were consistent with western blot experiment (Fig. 8C, Additional file 1: Fig. S14). In addition, Fe₃O₄-siPD-L1@M_{BV2} dose-dependently reduced the content of GSH in orthotopic drug-resistant GBM tissue. The GSH content in orthotopic drug-resistant GBM tissue in Fe₃O₄-siPD-L1@M_{BV2} + magnet group was lower in comparison with that in Fe₃O₄-siPD-L1@M_{BV2} group (Fig. 8D). Meanwhile, Fe₃O₄-siPD-L1@M_{BV2} dose-dependently increased the ROS level in orthotopic drug-resistant GBM tissue (Fig. 8C, E). Moreover, as compared with normal saline, Fe₃O₄-siNC and Fe₃O₄-siNC@M_{BV2} also significantly inhibited the GPX4 expression, GSH and ROS level in orthotopic drug-resistant GBM tissue, indicating that Fe₃O₄-siNC and Fe₃O₄-siNC@M_{BV2} induced ferroptosis and subsequently inhibited the growth of orthotopic drug-resistant glioma.

Thirdly, flow cytometer was used to investigate the effect of Fe₃O₄-siPD-L1@M_{BV2} on the maturation of DC cell in orthotopic drug-resistant GBM tissue. The proportion of CD11c⁺CD80⁺CD86⁺ in normal saline, Fe₃O₄-siPD-L1, Fe₃O₄-siPD-L1@M_{BV2} (0.3 mg/kg) and Fe₃O₄-siPD-L1@M_{BV2} (1 mg/kg) treatment groups was 1.57%, 7.8%, 17.84%, 19.26%, respectively. As compared with Fe₃O₄-siPD-L1@M_{BV2}, the proportion of matured DC cells in Fe₃O₄-siPD-L1@M_{BV2} + magnet group was significantly increased in orthotopic drug-resistant GBM tissue (Fig. 8F, Additional file 1: Fig. S15). Further study indicated that the proportion of CD3⁺CD8⁺IFN-γ⁺ T cells (T_{eff} cell) in orthotopic drug-resistant GBM tissue

(See figure on next page.)

Fig. 8 Effect of Fe₃O₄-siPD-L1@M_{BV2} on immune microenvironment and ferroptosis in orthotopic drug-resistant GBM tissue. **A** The protein expression of PD-L1, xCT and GPX4 in orthotopic drug-resistant GBM tissue detected by western blot. **B** Statistic analysis of PD-L1, xCT and GPX4 protein expression. **C** The protein expression of PD-L1, GPX4 and ROS level in orthotopic drug-resistant GBM tissue observed by immunofluorescence staining. **D** The content of GSH in orthotopic drug-resistant GBM tissue. **E** Statistic analysis of ROS level in orthotopic drug-resistant GBM tissue. **F** The ratio of matured DC cell in orthotopic drug-resistant GBM tissue. **G, H** The proportion of T_{eff} cell and T_{reg} cell in orthotopic drug-resistant GBM tissue. **I–M** The content of TNF-α, IFN-γ, IL-6, IL-10 and IL-12 in orthotopic drug-resistant GBM tissue. (n = 3, mean ± SD, *P < 0.05, **P < 0.01)

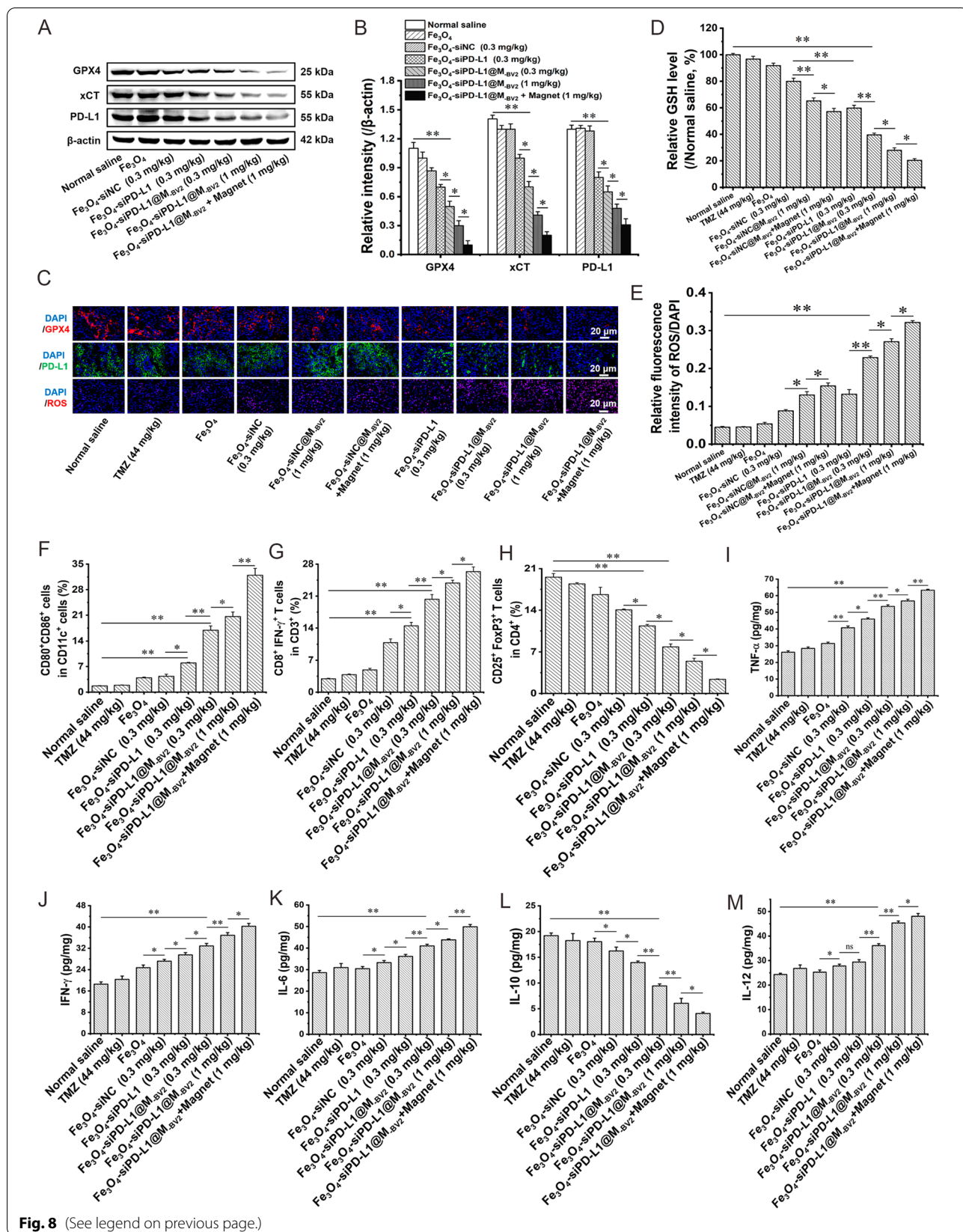


Fig. 8 (See legend on previous page.)

in normal saline, Fe₃O₄-siPD-L1, Fe₃O₄-siPD-L1@M_{BV2} (0.3 mg/kg) and Fe₃O₄-siPD-L1@M_{BV2} (1 mg/kg) treatment group was 3.10%, 13.43%, 19.25% and 23.1%, respectively. Fe₃O₄-siPD-L1@M_{BV2} + magnet obviously increased the number of T_{eff} cell in orthotopic drug-resistant GBM tissue as compared with Fe₃O₄-siPD-L1@M_{BV2} (Fig. 8G, Additional file 1: Fig. S16). The proportion of CD4⁺CD25⁺FoxP3⁺ T cells (T_{reg} cell) in orthotopic drug-resistant GBM tissue in normal saline, Fe₃O₄-siPD-L1, Fe₃O₄-siPD-L1@M_{BV2} (0.3 mg/kg) and Fe₃O₄-siPD-L1@M_{BV2} (1 mg/kg) treatment group was 18.76%, 11.05%, 7.24% and 5.29%, respectively. As compared with Fe₃O₄-siPD-L1@M_{BV2}, Fe₃O₄-siPD-L1@M_{BV2} + magnet markedly reduced the number of T_{reg} cell in orthotopic drug-resistant GBM tissue (Fig. 8H, Additional file 1: Fig. S17).

Finally, Fe₃O₄-siPD-L1@M_{BV2} dose-dependently increased the contents of TNF- α , IFN- γ , IL-6 and IL-12 but decreased the contents of IL-10 in orthotopic drug-resistant GBM cells. Fe₃O₄-siPD-L1@M_{BV2} + magnet significantly increased the contents of TNF- α , IFN- γ , IL-6 and IL-12 in comparison with Fe₃O₄-siPD-L1@M_{BV2} did (Fig. 8I–M). Moreover, immunofluorescence staining showed that a large amount of microglia was mainly distributed in orthotopic drug-resistant GBM tissue (Fig. 9A). Fe₃O₄-siPD-L1, Fe₃O₄-siPD-L1@M_{BV2} and Fe₃O₄-siPD-L1@M_{BV2} + magnet significantly increased the number of Iba-1⁺CD16/32⁺ cells (M1 type microglia) in drug-resistant GBM tissue in comparison with normal saline and Fe₃O₄-siNC. The number of Iba-1⁺CD16/32⁺ cells was the highest in Fe₃O₄-siPD-L1@M_{BV2} + magnet treatment group (Fig. 9B, C). Furthermore, as compared with normal saline and Fe₃O₄-siNC, Fe₃O₄-siPD-L1, Fe₃O₄-siPD-L1@M_{BV2} and Fe₃O₄-siPD-L1@M_{BV2} + magnet significantly reduced the number of Iba-1⁺CD206⁺ cells (M2 type microglia) in drug-resistant GBM tissue. The number of Iba-1⁺CD206⁺ cells was the lowest in Fe₃O₄-siPD-L1@M_{BV2} + magnet treatment group (Fig. 9B, D).

Preliminary safety evaluation of Fe₃O₄-siPD-L1@M_{BV2} in orthotopic drug-resistant GBM mice

On the 24th day after plantation of Luc-GL261/TR cell, H&E staining showed that no obvious abnormal morphological changes were observed in the heart, liver, spleen, lung and kidney in all treatment groups (Fig. 10A). Biochemical analysis further showed that ALT and AST activities, BUN and CREA contents in mice serum in each treatment group were all within the normal range (Fig. 10B–E).

Discussion

The PD-1/PD-L1 signaling pathway plays an important role in the tumor immune microenvironment [46]. The activation of PD-1/PD-L1 signaling pathway induces the apoptosis of the T_{eff} cell. Blocking the PD-1/PD-L1 signaling pathway activates T_{eff} cell, thus inhibiting tumor growth [47]. However, clinical data show that only less than 10% of patients with GBM response to immunotherapy because of the low immunogenicity of GBM [10, 48]. It has been shown that ferroptosis of cancer cells release high-mobility group box 1 (HMGB1) in an autophagy dependent manner [49], which increases the immunogenicity of cancer cells and promotes the maturation of DC cells [50–52]. The matured DC cells presents antigen to T lymphocytes and activates innate and adaptive immunity.

The key features of ferroptosis are the overload of Fe²⁺, depletion of GSH, the decrease of GPX4 activity and the consequent lipid peroxidation of cell membrane [53]. The results of MTT assay showed that Fe₃O₄-siPD-L1@M_{BV2} decreased GL261/TR cell activity in a concentration-dependent manner. However, the inhibitory effect of Fe₃O₄-siPD-L1@M_{BV2} on GL261/TR cell activity was significantly reduced in the present of ferroptosis inhibitors. After GL261/TR cells were incubated with Fe₃O₄-siPD-L1@M_{BV2}, the content of GSH and the protein expression of GPX4 in GL261/TR cells significantly decreased, which attenuated the ability of GL261/TR cells to clear intracellular ROS. This led to the increase of ROS level and lipid peroxidation in GL261/TR cells. However, in the present of ferroptosis inhibitor, the lipid peroxidation induced by Fe₃O₄-siPD-L1@M_{BV2} in GL261/TR cells was significantly attenuated. Moreover, in vivo experimental results indicated that as compared with Fe₃O₄, the GSH content and protein expression of GPX4 and xCT were markedly reduced, and the ROS level and Fe²⁺ content was significantly increased in orthotopic drug-resistant GBM tissue in Fe₃O₄-siPD-L1@M_{BV2} and Fe₃O₄-siPD-L1@M_{BV2} + magnet treatment group. Those results demonstrated that ferroptosis was involved in the inhibitory effect of Fe₃O₄-siPD-L1@M_{BV2} on GL261/TR cell activity. Fe₃O₄-siPD-L1@M_{BV2} induced the ferroptosis of orthotopic drug-resistant GBM cells by increasing Fe²⁺ content and reducing the GPX4 protein expression.

When Fe₃O₄-siPD-L1@M_{BV2} was co-cultured with GL261/TR cell, it significantly facilitated the maturation of DC cells. Ferroptosis inhibitors significantly inhibited the maturation of DC cells induced by Fe₃O₄-siPD-L1@M_{BV2}, suggesting that ferroptosis of GL261/TR cell induced by Fe₃O₄-siPD-L1@M_{BV2}

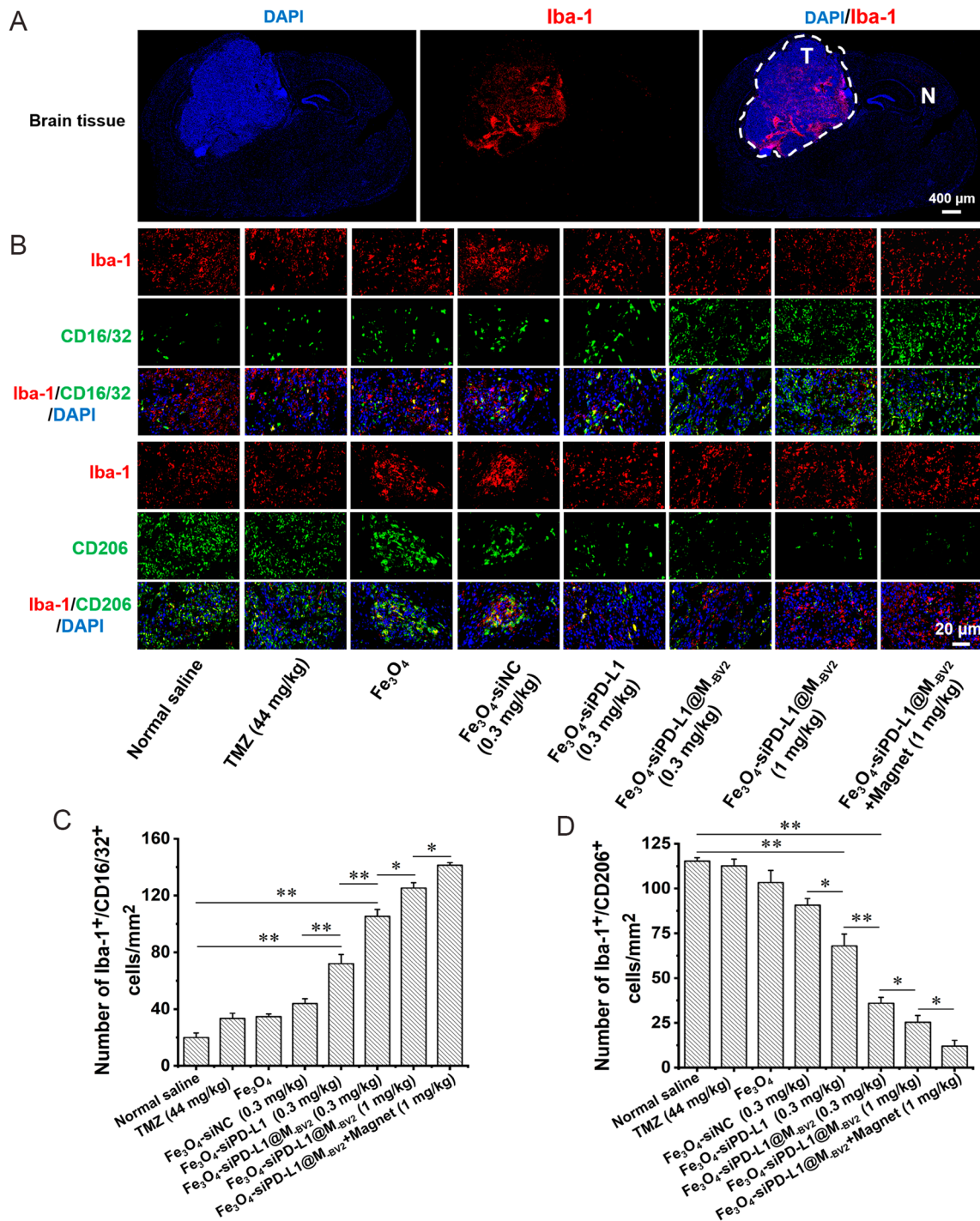


Fig. 9 Effect of Fe_3O_4 -siPD-L1@M_{BV2} on polarization of microglia in orthotopic drug-resistant GBM tissue. **A** Distribution of microglia (marked with Iba-1, red color) in orthotopic drug-resistant GBM tissue. T: tumor tissue; N: normal tissue. **B** M1-type microglia (Iba-1 and CD16/32 co-positive cells) and M2-type microglia (Iba-1 and CD206 co-positive cells) in orthotopic drug-resistant GBM tissue. **C, D** Statistic analysis of M1 type and M2 type microglia in orthotopic drug-resistant GBM tissue. (n = 3, mean \pm SD, * P < 0.05, ** P < 0.01)

promoted the maturation of DC cells. Meanwhile, the in vitro experiment indicated that IFN- γ significantly enhanced ferroptosis of GL261/TR cells and the maturation of DC cells induced by Fe₃O₄-siPD-L1@M_{BV2}. Moreover, the in vivo experiment indicated that IFN- γ content and the number of matured DC cells in orthotopic drug-resistant GBM tissue significantly increased in Fe₃O₄-siPD-L1@M_{BV2} group and Fe₃O₄-siPD-L1@M_{BV2} + magnet group. Fe₃O₄-siPD-L1@M_{BV2} reduced the protein expression of PD-L1 and increased the ratio between T_{eff} cell and T_{reg} cell in orthotopic drug-resistant GBM tissue. Those results suggested that T_{eff} cell was activated by Fe₃O₄-siPD-L1@M_{BV2} through blocking PD-1/PD-L1 signal pathway, resulting in the release of IFN- γ . IFN- γ released from activated T_{eff} cell enhanced the ferroptosis of Fe₃O₄-siPD-L1@M_{BV2}, which promoted the maturation of DC cells in orthotopic drug-resistant GBM tissue. This activated the T_{eff} cell in turn and subsequently inhibited the growth of orthotopic drug-resistant GBM.

Clinical studies have shown that there is a large number of microglia in GBM tissue [54, 55]. GBM tissue promotes the polarization of microglia toward anti-inflammatory M2 type [11]. Studies have also shown that PD-L1 antibody activate mice macrophages to secrete more TNF- α and IL-12, which induce polarization of macrophages toward a pro-inflammatory M1 type [56, 57]. The in vivo experimental results showed that Fe₃O₄-siPD-L1@M_{BV2} significantly increased the content of IFN- γ , TNF- α and IL-12 in orthotopic drug-resistant GBM tissue. The ratio between M1 type microglia and M2 type microglia in orthotopic drug-resistant GBM tissue was significantly increased by Fe₃O₄-siPD-L1@M_{BV2}. The above results demonstrated that Fe₃O₄-siPD-L1@M_{BV2} polarized M2 type microglia to M1 type microglia through increasing IFN- γ , TNF- α and IL-12 content in orthotopic drug-resistant GBM tissue.

Improving the stability in blood circulation and targeting to GBM is the key point for siPD-L1 to play its role in vivo. Pharmacokinetic results showed that Fe₃O₄-siPD-L1@M_{BV2} markedly increased the stability of siPD-L1 in blood. In vivo bioluminescence imaging results indicated that the coating of microglia membrane improved the brain targeting of Fe₃O₄ nanoparticles. LSCM observation indicated that Fe₃O₄-siPD-L1@M_{BV2} selectively distributed in the orthotopic drug-resistant GBM

tissue. In addition, as compared with Fe₃O₄-siPD-L1, the intracellular siPD-L1 in orthotopic drug-resistant GBM tissue was significantly increased after Fe₃O₄-siPD-L1@M_{BV2} was administrated. Meanwhile, the content of Fe²⁺ in orthotopic drug-resistant GBM tissue was also significantly increased by Fe₃O₄-siPD-L1@M_{BV2}. Those results demonstrated that Fe₃O₄-siPD-L1@M_{BV2} exhibited good targeting for orthotopic drug-resistant GBM tissue. siPD-L1 and Fe²⁺ were simultaneously delivered to orthotopic drug-resistant GBM by Fe₃O₄-siPD-L1@M_{BV2}. Due to the paramagnetism of Fe₃O₄ nanoparticle, the brain targeting rate and the accumulation of Fe₃O₄-siPD-L1@M_{BV2} in orthotopic drug-resistant GBM tissue was further increased under external magnetic field.

The in vivo imaging showed that Fe₃O₄-siPD-L1@M_{BV2} was mainly distributed in brain and liver, while less Fe₃O₄-siPD-L1@M_{BV2} was distributed in kidney and other tissue after intravenous administration. The amount of Fe₃O₄-siPD-L1@M_{BV2} in brain tissue reached its maximum value at 12 h after administration. The distribution of Fe₃O₄-siPD-L1@M_{BV2} in liver and brain significantly decreased at 24 h after administration. The above results indicated that Fe₃O₄-siPD-L1@M_{BV2} and Fe₃O₄-siPD-L1@M_{BV2} + magnet did not accumulate in the liver and kidney after a single tail vein injection. On the 24th day after plantation of Luc-GL261/TR cell, H&E staining and biochemical analysis indicated when Fe₃O₄-siPD-L1@M_{BV2} and Fe₃O₄-siPD-L1@M_{BV2} + magnet were intravenously injected into orthotopic drug-resistant GBM mice for 4 times within 12 days, they did not cause significant damage to heart, liver, spleen, lung and kidney in orthotopic drug-resistant GBM mice. However, this just was a preliminary safety evaluation. It is not certain yet if hepatorenal toxicity can be caused by Fe₃O₄-siPD-L1@M_{BV2} and Fe₃O₄-siPD-L1@M_{BV2} + magnet when its dose is greater than 1 mg/kg or more than 4 times of administration. This needs further study.

Western blot results showed that CX3CL1 and CSF-1 were highly expressed in GL261/TR cells, while CX3CR1 and CSF-1R were highly expressed in the membrane of microglia and surface of Fe₃O₄-siPD-L1 nanoparticles. In vitro studies showed that in the existence of chemokine CSF-1 and CX3CL1, the efficiency of Fe₃O₄-siPD-L1@M_{BV2} penetration in vitro BBB was significantly improved, and the accumulation of Fe₃O₄-siPD-L1@M_{BV2} in GL261/TR cells was

(See figure on next page.)

Fig. 10 Safety evaluation of Fe₃O₄-siPD-L1@M_{BV2} in orthotopic drug-resistant GBM mice. **A** H&E staining of heart, liver, spleen, lung and kidney tissue in orthotopic drug-resistant GBM mice. **B, C** Effects of Fe₃O₄-siPD-L1@M_{BV2} on ALT and AST activity in serum of orthotopic drug-resistant GBM mice. **D, E** Effects of Fe₃O₄-siPD-L1@M_{BV2} on content of BUN and CREA in serum of orthotopic drug-resistant GBM mice. The green area indicates the normal ranges. (n = 5, mean \pm SD)

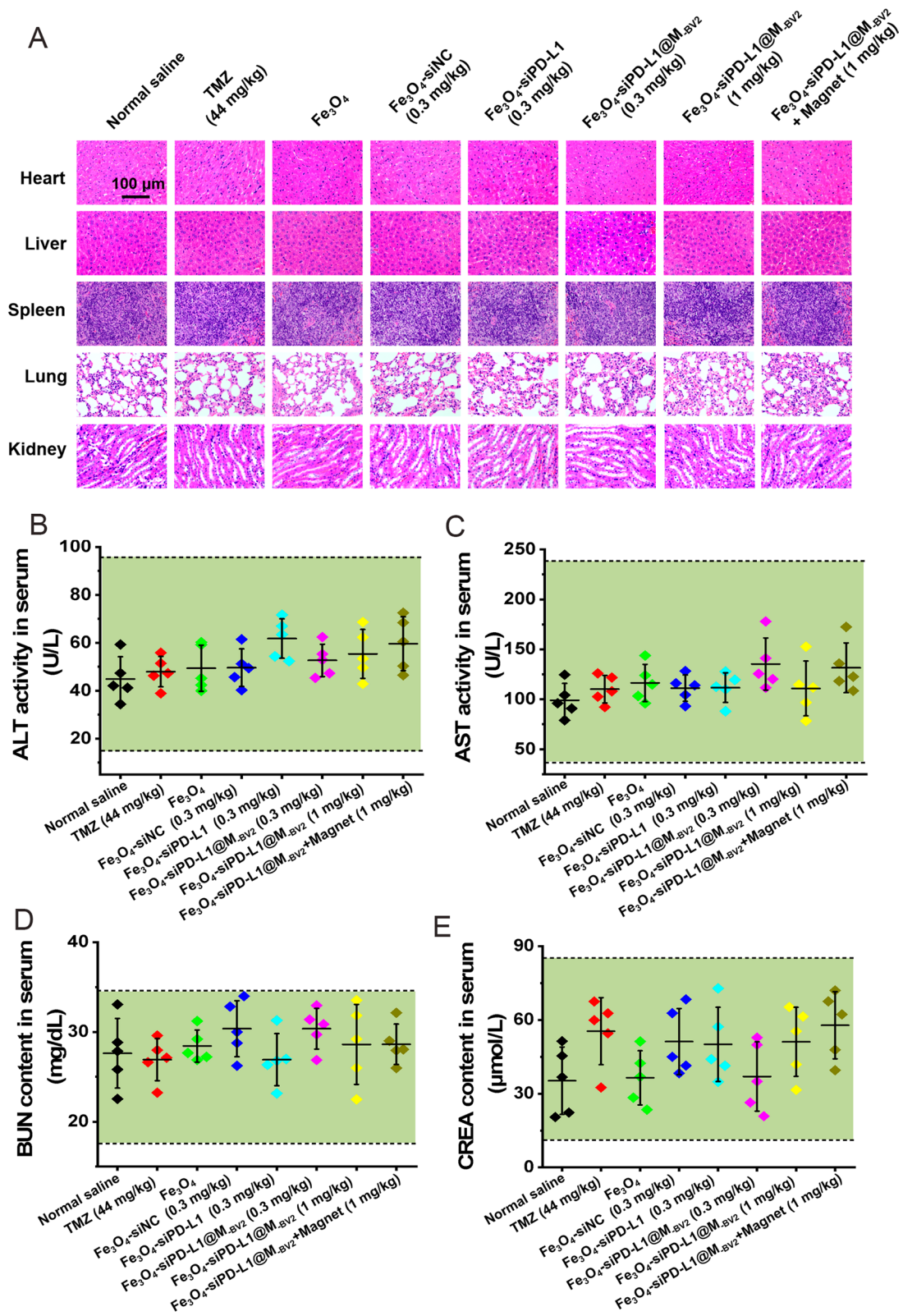


Fig. 10 (See legend on previous page.)

also markedly increased. In contrast, CSF-1 antibody, CX3CL1 antibody, CSF-1R antibody and CX3CR1 antibody significantly reduced the efficiency of Fe₃O₄-siPD-L1@M_{BV2} penetration in vitro BBB and its accumulation in GL261/TR cells. The results demonstrated that the interaction between chemokines (CSF-1 and CX3CL1) secreted by GL261/TR cells and receptors (CSF-1R and CX3CR1) on the microglia membrane promoted Fe₃O₄-siPD-L1@M_{BV2} to penetrate BBB and accumulate in GL261/TR cells.

Conclusion

Fe₃O₄-siPD-L1@M_{BV2} was actively delivered to orthotopic drug-resistant GBM cell through the interaction between microglia membrane and GBM cell. Fe₃O₄-siPD-L1@M_{BV2} activated T_{eff} cell by blocking the PD-1/PD-L1 signaling pathway. The activated T_{eff} cell released IFN-γ to promote ferroptosis of GBM cells and subsequently facilitated the maturation of DC cells in orthotopic drug-resistant GBM tissue. The matured DC cells presented GBM antigens to T lymphocytes to activate T_{eff} cell in turn. Meanwhile, M2 type microglia was polarized to M1 type microglia by IFN-γ secreted via T_{eff} cell in orthotopic drug-resistant GBM tissue. Finally, a virtuous cycle between ferroptosis and immunotherapy was formed and promoted each other by Fe₃O₄-siPD-L1@M_{BV2}, which exerted a synergistic effect on the treatment of orthotopic drug-resistant GBM.

Abbreviations

ALT: Alanine aminotransferase; AST: Aspartate aminotransferase; BBB: Blood brain barrier; BODIPY-C11: Boron difluoride pyrrole fluorescent dyes-C11; BUN: Urea nitrogen; BSA: Bovine albumin; CD11c-APC: Clusters of differentiation 11 c-Allophycocyanin; CD25-FITC: Clusters of differentiation 25-fluorescein isothiocyanate; CD3-APC: Clusters of differentiation 3-Allophycocyanin; CD4-PE-Cy7: Clusters of differentiation 4-Phycoerythrin-Sulfo-Cyanine7; CD44: Clusters of differentiation 44; CD8-FITC: Clusters of differentiation 8-fluorescein isothiocyanate; CD80-FITC: Clusters of differentiation 80-fluorescein; CD86-PE: Clusters of differentiation 86-Phycoerythrin; CREA: Creatinine; CX3CL1: C-X3-C motif chemokine ligand 1; CX3CR1: C-X3-C motif chemokine receptor 1; DAPI: 4',6-Diamidino-2-phenylindole dihydrochloride; DFO: Deferoxamine; DHE: Dihydroethidium; DMEM: Dulbecco's modified eagle medium; DMSO: Dimethyl sulfoxide; E-cadherin: E-Ca²⁺ dependent cell adhesion molecules; FoxP3-PE: Forkhead box P3-Phycoerythrin; Fer-1: Ferrostatin-1; GL261/TR: TMZ-resistant glioma cells; GSH: Glutathione; GM-CSF: Granulocyte-macrophage colony stimulating factor; GPX4: Glutathione Peroxidase 4; HMGB1: Human high-mobility group box-1; Iba-1: Ionized calcium binding adaptor molecule 1; HR: Hemolysis rate; Iba-1: Ionized calcium binding adaptor molecule 1; IL-6/10/12: Interleukin-6/10/12; IFN-γ: Interferon-γ; IFN-γ-PE-Cy7: Interferon-γ-Phycoerythrin-Sulfo-Cyanine7; LPO: Lipid peroxidation; LSM: Laser scanning confocal microscopy; M_{BV2}: Microglial cell membrane; MGMT: O⁶-methylguanine-DNA-methyltransferase; MMP-9: Matrix metalloproteinases-9; MTT: 3-(4,5-Dimethylthiazol-2-yl)-2,5-diphenyltetrazolium bromide; N-cadherin: N-Ca²⁺ dependent cell adhesion molecules; PBS: Phosphate buffer saline; PDI: Polydispersity index; PD-L1: Programmed cell death ligand-1; ROS: Reactive oxygen species; RPMI1640: Roswell Park Memorial Institute 1640; SDS-PAGE: Sulfate-polyacrylamide gel electrophoresis; TEM: Transmission electron microscope; TGF-β: Transforming growth factor-β; TNF-α: Tumor necrosis factor-α; Tris: Trimethylol aminomethane; xCT: Cystine/glutamic acid reverse transporter.

Supplementary Information

The online version contains supplementary material available at <https://doi.org/10.1186/s12951-022-01360-6>.

Additional file 1: Figure S1. Diagram of the applied magnetic field in orthotopic drug-resistant GBM mice brain after Fe₃O₄-siPD-L1@M_{BV2} was injected into the tail vein. **Figure S2.** Characterization of Fe₃O₄-siPD-L1@M_{BV2}. (A) Element mapping analysis diagram of Fe₃O₄. (B) The zeta potential of Fe₃O₄, Fe₃O₄-siPD-L1, M_{BV2} and Fe₃O₄-siPD-L1@M_{BV2}. (C) Stability of Fe₃O₄-siPD-L1@M_{BV2} in water, PBS and 10% FBS solution. (D) TEM image of Fe₃O₄. (E) TEM image of Fe₃O₄-siPD-L1@M_{BV2}. (F) Hemolysis phenomenon of Fe₃O₄-siPD-L1@M_{BV2}. (G) Statistic analysis of hemolysis of Fe₃O₄-siPD-L1@M_{BV2}. (n = 3, mean ± SD). **Figure S3.** The density of GL261/TR cells, HT-22 cells, BV2 cells and RAW264.7 cells after the cells incubated at 37 °C for 24 h. (A) The density of GL261/TR cells, HT-22 cells, BV2 cells and RAW264.7 cells observed by optical microscope. (B) The density of GL261/TR cells, HT-22 cells, BV2 cells and RAW264.7 cells counted by using cell counters. (n = 3, mean ± SD, ns: no significant difference). **Figure S4.** Statistic analysis of Fe₃O₄-FAM@M_{BV2} uptake by GL261/TR cells, HT-22 cells, BV2 cells and RAW264.7 cells detected by flow cytometer (n = 3, mean ± SD, *P < 0.05, **P < 0.01, ns: no significant difference). **Figure S5.** The uptake mechanism of Fe₃O₄-FAM@M_{BV2} on GL261/TR cells detected by flow cytometer. (A) Effects of different inhibitors on the uptake of Fe₃O₄-FAM@M_{BV2} by GL261/TR cells. (B) Statistic analysis of Fe₃O₄-FAM@M_{BV2} uptake by GL261/TR cells (n = 3, mean ± SD, **P < 0.01). **Figure S6.** The effect of Fe₃O₄-siPD-L1@M_{BV2} on protein expression of PD-L1 in GL261 cells. (n = 3, mean ± SD, *P < 0.05, **P < 0.01). **Figure S7.** The effect of Fe₃O₄-siPD-L1@M_{BV2} on the viability of GL261/TR cells. (A) The effect of Fe₃O₄-siPD-L1@M_{BV2} on the death and living GL261/TR cells. (B) Statistic analysis of death and living GL261/TR cells. (n = 3, mean ± SD, *P < 0.05, **P < 0.01, ns: no significant difference). **Figure S8.** The effect of IFN-γ on the xCT protein expression in GL261/TR cells. (n = 3, mean ± SD, **P < 0.01). **Figure S9.** The resistance values between transwell donor chamber and recipient chamber within 12 h after drug administration. (n = 3, mean ± SD, ns: no significant difference). **Figure S10.** Statistic analysis of Fe₃O₄-FAM@M_{BV2} uptake by GL261/TR cells after Fe₃O₄-FAM@M_{BV2} penetrated in vitro BBB detected by flow cytometer. (n = 3, mean ± SD, **P < 0.01). **Figure S11.** The distribution of Fe₃O₄-siPD-L1@M_{BV2} in organs of orthotopic drug-resistant GBM mice observed by in vivo bioluminescence imaging. **Figure S12.** The effect of Fe₃O₄-siPD-L1@M_{BV2} on body weight of orthotopic drug-resistant GBM mice. (n = 10, mean ± SD). **Figure S13.** The expression of invasion-related proteins in orthotopic drug-resistant GBM tissue after orthotopic drug-resistant GBM mice was treated with Fe₃O₄-siPD-L1@M_{BV2}. (A) The expression of invasion-related proteins in orthotopic drug-resistant GBM tissue detected by western blot. (B) Semi-quantitative analysis of invasion-related proteins. (n = 3, mean ± SD, *P < 0.05, **P < 0.01). **Figure S14.** Effect on the protein expression of GPX4 and PD-L1 in orthotopic drug-resistant GBM tissue after orthotopic drug-resistant GBM mice was treated with Fe₃O₄-siPD-L1@M_{BV2}. (A) Semi-quantitative analysis of GPX4 protein expression in orthotopic drug-resistant GBM tissue detected by immunofluorescence staining. (B) Semi-quantitative analysis of PD-L1 protein expression in orthotopic drug-resistant GBM tissue. (n = 3, mean ± SD, *P < 0.05, **P < 0.01, ns: no significant difference). **Figure S15.** Typical flow cytometric graph of the matured DC cells. **Figure S16.** Typical flow cytometric graph of CD3⁺CD8⁺IFN-γ⁺ T cells. **Figure S17.** Typical flow cytometric graph of CD4⁺CD25⁺FoxP3⁺ T cells.

Authors' contributions

BL, DL, and SZ conceived the manuscript. BL wrote the first draft. DL and SZ revised the first draft. BL and QJ performed the experiments. YC, ML, BZ, and QM provided grouping suggestions. All of the authors have read and approved the final manuscript.

Funding

This work was financially supported by the National Natural Science Foundation of China (81872803, 82073775), Shaanxi Province Key Research and Development Projects of China (2021ZDLSF03-08) and Shaanxi Natural Science Foundation (2020JQ-458).

Availability of data and materials

All data generated or analyzed during this study are included in this published article and its supplementary information file.

Declarations**Ethics approval and consent to participate**

All animal experiments were approved by the Air Force Medical University Institutional Animal Care and Utilization Committee (No: IACUC-20210403).

Consent for publication

Not applicable.

Competing interests

There is no competing interest.

Author details

¹Department of Pharmaceutics, School of Pharmacy, Air Force Medical University, Changle West Road 169, Xi'an 710032, Shaanxi, China. ²Key Laboratory of Gastrointestinal Pharmacology of Chinese Materia Medica of the State Administration of Traditional Chinese Medicine, Department of Pharmacology, School of Pharmacy, Air Force Medical University, Changle West Road 169, Xi'an 710032, Shaanxi, China.

Received: 3 December 2021 Accepted: 8 March 2022

Published online: 27 March 2022

References

- Ma Y, Zhang J, Rui Y, Rolle J, Xu T, Qian Z, et al. Depletion of glioma stem cells by synergistic inhibition of mtor and c-myc with a biological camouflaged cascade brain-targeting nanosystem. *Biomaterials*. 2021;268:120564.
- Zou Y, Sun X, Wang Y, Yan C, Liu Y, Li J, et al. Single siRNA nanocapsules for effective siRNA brain delivery and glioblastoma treatment. *Adv Mater*. 2020;32:2000416.
- Awah C U, Winter J, Mazdoom C M, Ogunwobi O O. Nsun6, an RNA methyltransferase of 5-mc controls glioblastoma response to temozolomide (TMZ) via nelfb and rps6kb2 interaction. *Cancer Biol Ther*. 2021;1–11.
- Wu S, Li X, Gao F, de Groot JF, Koul D, Yung W. Parp-mediated parylation of MGMT is critical to promote repair of temozolomide-induced o6-methylguanine DNA damage in glioblastoma. *Neuro Oncol*. 2021;23:920–31.
- Dey A, Islam S, Patel R, Acevedo-Duncan M. The interruption of atypical PKC signaling and temozolomide combination therapy against glioblastoma. *Cell Signal*. 2021;77:109819.
- Wei Y, Lu C, Zhou P, Zhao L, Lyu X, Yin J, et al. EIF4A3-induced circular RNA ASAP1 promotes tumorigenesis and temozolomide resistance of glioblastoma via NRAS/MEK1/ERK1–2 signaling. *Neuro Oncol*. 2021;23:611–24.
- Liang P, Wang G, Liu X, Wang Z, Wang J, Gao W. Spatiotemporal combination of thermosensitive polypeptide fused interferon and temozolomide for post-surgical glioblastoma immunochemotherapy. *Biomaterials*. 2021;264:120447.
- Zheng C, Song Q, Zhao H, Kong Y, Sun L, Liu X, et al. A nanoplatform to boost multi-phases of cancer-immunity-cycle for enhancing immunotherapy. *J Control Release*. 2021;339:403–15.
- Shu C, Li Q. Current advances in pd-1/pd-l1 axis-related tumour-infiltrating immune cells and therapeutic regimens in glioblastoma. *Crit Rev Oncol/Hematol*. 2020;151:102965.
- Jackson CM, Choi J, Lim M. Mechanisms of immunotherapy resistance: lessons from glioblastoma. *Nat Immunol*. 2019;20:1100–9.
- Wang X, Guo G, Guan H, Yu Y, Lu J, Yu J. Challenges and potential of pd-1/pd-l1 checkpoint blockade immunotherapy for glioblastoma. *J Exp Clin Canc Res*. 2019. <https://doi.org/10.1186/s13046-019-1085-3>.
- Agliardi G, Liuzzi AR, Hotblack A, De Feo D, Núñez N, Stowe CL, et al. Intratumoral IL-12 delivery empowers CAR-T cell immunotherapy in a pre-clinical model of glioblastoma. *Nat Commun*. 2021;12:444.
- Amoozgar Z, Kloepfer J, Ren J, Tay RE, Kazer SW, Kiner E, et al. Targeting Treg cells with GITR activation alleviates resistance to immunotherapy in murine glioblastomas. *Nat Commun*. 2021;12:2582.
- Grabowski MM, Sankey EW, Ryan KJ, Chongsathidkiet P, Lorrey SJ, Wilkinson DS, et al. Immune suppression in gliomas. *J Neurooncol*. 2021;151:3–12.
- Lanza M, Casili G, Campolo M, Paterniti I, Colarossi C, Mare M, et al. Immunomodulatory effect of microglia-released cytokines in gliomas. *Brain Sci*. 2021. <https://doi.org/10.3390/brainsci11040466>.
- Magana-Maldonado R, Chavez-Cortez EG, Olascoaga-Arellano NK, Lopez-Mejia M, Maldonado-Leal FM, Sotelo J, et al. Immunological evasion in glioblastoma. *Biomed Res Int*. 2016;2016:7487313.
- Li K, Xu K, He Y, Lu L, Mao Y, Gao P, et al. Functionalized tumor-targeting nanosheets exhibiting Fe(II) overloading and GSH consumption for ferroptosis activation in liver tumor. *Small*. 2021;17:2102046.
- Hassannia B, Vandenabeele P, Vanden BT. Targeting ferroptosis to iron out cancer. *Cancer Cell*. 2019;35:830–49.
- Wang W, Green M, Choi JE, Gijón M, Kennedy PD, Johnson JK, et al. Cd8+ T cells regulate tumour ferroptosis during cancer immunotherapy. *Nature*. 2019;569:270–4.
- Weiland A, Wang Y, Wu W, Lan X, Han X, Li Q, et al. Ferroptosis and its role in diverse brain diseases. *Mol Neurobiol*. 2019;56:4880–93.
- Wang D, Wang T, Yu H, Feng B, Zhou L, Zhou F, et al. Engineering nanoparticles to locally activate T cells in the tumor microenvironment. *Sci Immunol*. 2019. <https://doi.org/10.1126/sciimmunol.aau6584>.
- Sheng S, Liu F, Lin L, Yan N, Wang Y, Xu C, et al. Nanozyme-mediated cascade reaction based on metal-organic framework for synergetic chemo-photodynamic tumor therapy. *J Control Release*. 2020;328:631–9.
- Cloughesy TF, Mochizuki AY, Orpilla JR, Hugo W, Lee AH, Davidson TB, et al. Neoadjuvant anti-pd-1 immunotherapy promotes a survival benefit with intratumoral and systemic immune responses in recurrent glioblastoma. *Nat Med*. 2019;25:477–86.
- Jiang Q, Wang K, Zhang X, Ouyang B, Liu H, Pang Z, et al. Platelet membrane-camouflaged magnetic nanoparticles for ferroptosis-enhanced cancer immunotherapy. *Small*. 2020;16:2001704.
- Yost KE, Chang HY, Satpathy AT. Recruiting T cells in cancer immunotherapy. *Science (American Association for the Advancement of Science)*. 2021;372:130–1.
- Liang H, Wu X, Zhao G, Feng K, Ni K, Sun X. Renal clearable ultrasmall single-crystal Fe nanoparticles for highly selective and effective ferroptosis therapy and immunotherapy. *J Am Chem Soc*. 2021;143:15812–23.
- Subhan MA, Torchilin VP. SiRNA based drug design, quality, delivery and clinical translation. *Nanomed Nanotechnol Biol Med*. 2020;29:102239.
- Mousazadeh H, Pilehvar-Soltanahmadi Y, Dadashpour M, Zarghami N. Cyclodextrin based natural nanostructured carbohydrate polymers as effective non-viral siRNA delivery systems for cancer gene therapy. *J Control Release*. 2021;330:1046–70.
- Ding L, Tang S, Wyatt TA, Knoell DL, Oupicky D. Pulmonary siRNA delivery for lung disease: review of recent progress and challenges. *J Control Release*. 2021;330:977–91.
- Zhang Y, Fu X, Jia J, Wikerholmen T, Xi K, Kong Y, et al. Glioblastoma therapy using codelivery of cisplatin and glutathione peroxidase targeting siRNA from iron oxide nanoparticles. *ACS Appl Mater Interfaces*. 2020;12:43408–21.
- Soetaert F, Korangath P, Serantes D, Fiering S, Ivkov R. Cancer therapy with iron oxide nanoparticles: agents of thermal and immune therapies. *Adv Drug Deliv Rev*. 2020;163–164:65–83.
- Maurer V, Altin S, Ag SD, Zarinwall A, Temel B, Vogt PM, et al. In-vitro application of magnetic hybrid niosomes: targeted siRNA-delivery for enhanced breast cancer therapy. *Pharmaceutics*. 2021. <https://doi.org/10.3390/pharmaceutics13030394>.
- Lopez-Barbosa N, Garcia JG, Cifuentes J, Castro LM, Vargas F, Ostos C, et al. Multifunctional magnetite nanoparticles to enable delivery of siRNA for the potential treatment of Alzheimer's. *Drug Deliv*. 2020;27:864–75.
- Zhang T, Xu Q, Huang T, Ling D, Gao J. New insights into biocompatible iron oxide nanoparticles: a potential booster of gene delivery to stem cells. *Small*. 2020;16:2001588.
- Israel LL, Galstyan A, Holler E, Ljubimova JY. Magnetic iron oxide nanoparticles for imaging, targeting and treatment of primary and metastatic tumors of the brain. *J Control Release*. 2020;320:45–62.
- Furtado D, Björnmalm M, Ayton S, Bush AI, Kempe K, Caruso F. Overcoming the blood–brain barrier: the role of nanomaterials in treating neurological diseases. *Adv Mater*. 2018;30:1801362.

37. Qiao S, Cheng Y, Liu M, Ji Q, Zhang B, Mei Q, et al. Chemoattractants driven and microglia based biomimetic nanoparticle treating TMZ-resistant glioblastoma multiforme. *J Control Release*. 2021;336:54–70.
38. Gutmann DH, Kettenmann H. Microglia/brain macrophages as central drivers of brain tumor pathobiology. *Neuron*. 2019;104:442–9.
39. Hambardzumyan D, Gutmann DH, Kettenmann H. The role of microglia and macrophages in glioma maintenance and progression. *Nat Neurosci*. 2016;19:20–7.
40. Gong T, Cai Y, Sun F, Chen J, Su Z, Shuai X, et al. A nanodrug incorporating sirna pd-I1 and birinapant for enhancing tumor immunotherapy. *Biomater Sci*. 2021. <https://doi.org/10.1039/D1BM01299A>.
41. Chatterjee S, Chatterjee A, Jana S, Dey S, Roy H, Das MK, et al. Transforming growth factor beta orchestrates PD-I1 enrichment in tumor-derived exosomes and mediates cd8 T-cell dysfunction regulating early phosphorylation of TCR signalome in breast cancer. *Carcinogenesis*. 2021;42:38–47.
42. Likittrakulwong W, Poolprasert P, Srikaeo K. Effects of extraction methods on protein properties obtained from paddy rice and germinated paddy rice. *PeerJ*. 2021;9: e11365.
43. Korolev D, Shumilo M, Shulmeyster G, Krutikov A, Golovkin A, Mishanin A, et al. Hemolytic activity, cytotoxicity, and antimicrobial effects of human albumin- and polysorbate-80-coated silver nanoparticles. *Nanomaterials (Basel)*. 2021. <https://doi.org/10.3390/nano11061484>.
44. Sun C, Lu J, Wang J, Hao P, Li C, Qi L, et al. Redox-sensitive polymeric micelles with aggregation-induced emission for bioimaging and delivery of anticancer drugs. *J Nanobiotechnol*. 2021;19:14.
45. Andersson EA, Rocha-Ferreira E, Hagberg H, Mallard C, Ek CJ. Function and biomarkers of the blood-brain barrier in a neonatal germinal matrix haemorrhage model. *Cells-Basel*. 2021;10:1677.
46. Setordzi P, Chang X, Liu Z, Wu Y, Zuo D. The recent advances of pd-1 and pd-I1 checkpoint signaling inhibition for breast cancer immunotherapy. *Eur J Pharmacol*. 2021;895: 173867.
47. Munari E, Mariotti FR, Quatrini L, Bertoglio P, Tumino N, Vacca P, et al. Pd-1/pd-I1 in cancer: pathophysiological, diagnostic and therapeutic aspects. *Int J Mol Sci*. 2021. <https://doi.org/10.3390/ijms22105123>.
48. Xu S, Tang L, Li X, Fan F, Liu Z. Immunotherapy for glioma: current management and future application. *Cancer Lett*. 2020;476:1–12.
49. Jia L, Song H, Fan W, Song Y, Wang G, Li X, et al. The association between high mobility group box 1 chromatin protein and mitotic chromosomes in glioma cells. *Oncol Lett*. 2020;19:745–52.
50. Chen X, Yan L, Jiang F, Lu Y, Zeng N, Yang S, et al. Identification of a ferroptosis-related signature associated with prognosis and immune infiltration in adrenocortical carcinoma. *Int J Endocrinol*. 2021;2021:4654302.
51. Zhu M, Yang M, Zhang J, Yin Y, Fan X, Zhang Y, et al. Immunogenic cell death induction by ionizing radiation. *Front Immunol*. 2021;12: 705361.
52. Muraio A, Aziz M, Wang H, Brenner M, Wang P. Release mechanisms of major dampers. *Apoptosis*. 2021;26:152–62.
53. Liu J, Kuang F, Kroemer G, Klionsky DJ, Kang R, Tang D. Autophagy-dependent ferroptosis: machinery and regulation. *Cell Chem Biol*. 2020;27:420–35.
54. Ma J, Chen CC, Li M. Macrophages/microglia in the glioblastoma tumor microenvironment. *Int J Mol Sci*. 2021. <https://doi.org/10.3390/ijms22115775>.
55. Zhang Q, Wang J, Yao X, Wu S, Tian W, Gan C, et al. Programmed cell death 10 mediated cxcl2-cxcr2 signaling in regulating tumor-associated microglia/macrophages recruitment in glioblastoma. *Front Immunol*. 2021;12: 637053.
56. Su S, Zhao J, Xing Y, Zhang X, Liu J, Ouyang Q, et al. Immune checkpoint inhibition overcomes ADCP-induced immunosuppression by macrophages. *Cell*. 2018;175:442–57.
57. Hartley GP, Chow L, Ammons DT, Wheat WH, Dow SW. Programmed cell death ligand 1 (pd-I1) signaling regulates macrophage proliferation and activation. *Cancer Immunol Res*. 2018;6:1260–73.

Publisher's Note

Springer Nature remains neutral with regard to jurisdictional claims in published maps and institutional affiliations.

Ready to submit your research? Choose BMC and benefit from:

- fast, convenient online submission
- thorough peer review by experienced researchers in your field
- rapid publication on acceptance
- support for research data, including large and complex data types
- gold Open Access which fosters wider collaboration and increased citations
- maximum visibility for your research: over 100M website views per year

At BMC, research is always in progress.

Learn more biomedcentral.com/submissions

